



# Enhanced wideband low-frequency sound absorption of a single-layer multiple parallel-arranged inhomogeneous microperforated panel absorber

Faisal Rafique<sup>1</sup> · Jiu Hui Wu<sup>1</sup> · Syed Murawat Abbas Naqvi<sup>2,3</sup> · Fuyin Ma<sup>1</sup>

Received: 2 July 2021 / Accepted: 16 August 2021 / Published online: 26 August 2021  
© Australian Acoustical Society 2021

## Abstract

A single layer of four parallel-arranged inhomogeneous microperforated panels (iMPP) absorber is proposed to achieve low-frequency sound absorption and wider frequency bandwidth. The hole diameter of the four parallel-arranged iMPP is set to be equal to or less than 1 mm. The theoretical formula for calculating the absorption coefficient under normal incident sound is established based on an electrical equivalent circuit model (ECM). The parametric study has been performed on the MATLAB software, and the expected results are obtained. The results indicate that the proposed model can produce a wider absorption bandwidth of 195–455 Hz in the low-frequency region with an average absorption coefficient of more than 90% ( $\alpha=0.91$ ). To achieve the desired effect, the absorption coefficient and the bandwidth can be tuned by adjusting the aperture size, perforation ratio, thickness of iMPP with depth and width of the back cavity. Also, it is found that iMPP can produce wider bandgaps with good absorption peaks in the low-frequency region by designing sub-MPP of smaller hole diameter, large perforation ratio, and with large cavity depths and the sub-MPP of large hole diameter, small perforation ratio, and with short cavity depths. The finite element method has been employed on COMSOL Multiphysics 5.5a to simulate the acoustic absorption performance of the model and compared with the ECM-based predicted and square impedance tube-based experimental results. Compared with other homogeneous MPPs of different arrangements, this absorber provides exceptional absorption performance in a low-frequency range due to its lightweight structure, and convenient manufacturing availability, this enhanced form of iMPP absorber has great potential in acoustics and noise control applications.

**Keywords** Microperforated panel (MPP) · Low-frequency · Absorption coefficient · Inhomogeneous MPP (iMPP) · Square impedance tube · Liquid crystal display (LCD) · 3D printing

## 1 Introduction

Microperforated panel (MPP) absorbers are important for noise control applications in recent times due to their unique and attractive properties. Also, as a substitute for conventional fibrous and porous sound-absorbing materials, it is

widely used as broadband sound-absorbing materials when noise and environmental safety are of the highest priority [1–3]. When a sound field is imposed, the MPP operates on a mechanism similar to that of the Helmholtz resonator in which the MPP is positioned in front of firm support separated by an air cavity. Compared to other resonance-based sound absorption materials, the MPP absorber can provide a good bandwidth of absorption close to resonance due to the presence of a sub-millimeter perforation.

The absorption peak frequency and bandwidth of the MPP can be controlled and changed by manipulating the parameters of the MPP, such as aperture, thickness, perforation ratio, and cavity depth. Since MPP can be made from solid panels, its optical properties add esthetic value and provide an attractive indoor appearance. High-cost manufacturing technology makes the wide use of microperforated panels in low-frequency noise control vulnerable, so there

✉ Jiu Hui Wu  
ejhwu@mail.xjtu.edu.cn

<sup>1</sup> School of Mechanical Engineering and State Key Laboratory for Strength and Vibration of Mechanical Structures, Xi'an Jiaotong University, Xi'an 710049, China

<sup>2</sup> Key Laboratory of Thermo-Fluid Science and Engineering, MOE, Xi'an Jiaotong University, Xi'an 710049, China

<sup>3</sup> Mechanical Engineering Department, NFC(IEFR), Faisalabad, Pakistan

is a need to find cheaper and more efficient ways to manufacture MPPs. In a study, Zha et al. [4] designed a parallel structure with two dissimilar cavities, and its normal incident absorption coefficient is measured by impedance tube. There were different resonance peaks due to the different depths of the cavity. To present additional resonance, an arrangement of parallel or series extended structures based on the MPP was proposed. A combination of double-layer or multi-layer MPPs with a roundly arranged back-air cavity in the direction of acoustic wave propagation is proposed [2, 5–8]. The results show that, with the increase in air cavity, the absorption bandwidth is extended to a low frequency due to the addition of the resonance peak. The introduction of multiple resonances through the composite MPP absorption array is another way of expanding the absorption bandwidth. Then, two different combinations of MPP absorbers were proposed by Sakagami et al. [9] to obtain a broadband absorption device, in which the same MPP has different cavity depth or different MPP has the same-cavity depth. Absorption characteristics were defined by considering the excessive attenuation caused by impedance disruption. Wang et al. [10] deliberated the physical absorption mechanism of MPP absorber array consists of three microperforated panel absorbers with dissimilar cavity depth. They determined a strong local resonance due to the frequency shift caused by the internal resonator interface and the dissimilar resonance matching conditions of the MPP absorber. In addition to numerical and experimental studies on the diagonal incidence sound absorption of four parallel-arranged MPP absorbers in the diffusion field [11]. Some studies have suggested improving bandwidth absorption of MPP in the low-frequency region. Improvements to the traditional single-layer MPP were proposed, including the installation of a honeycomb structure behind the MPP [12, 13], the structure of tapered holes [14, 15], the size of the hole (diameter) is greatly reduced to extra-micro size [16], and including of parallel elongated tubes [17, 18]. Mosa [19] introduced inhomogeneous perforation and was limited to only two subsections behind iMPP and bandwidth in the higher frequency region. For low-frequency sound absorption, Li et al. [20] examined a parallel-arranged perforated panel absorber, in which the number of perforations was fewer and hence easier to be produced in contrast with that of MPP.

This particular study further extends the inhomogeneous perforation work in [19], with its innovative thin squared-shaped structure (less than 1 mm thickness), different hole diameters of 0.7–1 mm, dissimilar cavity widths and depths with partition and different perforation ratios have been designed to enhance low-frequency sound absorption with a wider bandwidth. Furthermore, to anticipate the absorption coefficient of the system, Maa's [1] formulation, which is based on the electrical equivalent circuit (ECM) method, is used to derive a mathematical model. MATLAB

software-based parametric study has been performed to obtain predicted results based on a mathematical model. In this paper, the working frequency of 10 Hz up to 1000 Hz under normal incidence is used to present the performance of iMPP. The iMPP layer was manufactured using additive manufacturing (Liquid crystal display-LCD) technology. A single-layer four parallel-arranged iMPP with an air cavity was studied. Absorption performance was numerically and experimentally measured using FEM simulation and square impedance tube, respectively. The interpretation of the current study is better than that of previous studies is more feasible due to its lightweight and thin structure, which was lacking in previous studies, particularly for low-frequency sound absorption.

This paper is organized as follows: in Sect. 2, a mathematical model of a specific assembly comprising of four inhomogeneous microperforated panels (iMPP) arranged in parallel is illustrated; in Sect. 3, the effect of different parameters on the absorption coefficient and their simulation results are specified; in Sect. 4, FEM simulation in COMSOL Multiphysics 5.5a has been performed; in Sect. 5, the experimental validation is presented which is in a decent agreement with predicted results followed by the conclusions in Sect. 6.

## 2 Theoretical Considerations

### 2.1 The Impedance of the Microperforated Panel

Maa [5], first proposed the basic structure and concept of the MPP absorber. A single microperforated panel absorber comprises of thickness 't', perforation holes of  $\leq 1$  mm, followed by a stiff wall with an air cavity of depth, D. A MPP's specific acoustic impedances ( $Z_{MPP}$ ) is comprised of a real part ( $Z_{resistance}$ ) and an imaginary part ( $Z_{reactance}$ ) given by

$$Z_{MPP} = Z_{resistance} + Z_{reactance} = r + j\omega m \quad (1)$$

with

$$r = \frac{32\eta t}{\rho c d^2 p} \left( \sqrt{1 + \frac{k^2}{32}} + \frac{kd\sqrt{2}}{8t} \right) \quad (2)$$

$$m = \frac{t}{\rho c} \left( 1 + \left( 9 + \frac{k^2}{2} \right)^{-1/2} + \frac{0.85d}{t} \right) \quad (3)$$

where  $k = d/2\sqrt{\omega\rho/\eta}$ , perforation ratio  $p = (\pi/4) * (d/b)^2$ ,  $d$  is the diameter of the holes, the density of air  $\rho = 1.2\text{kg/m}^3$ , speed of sound  $c = 344$  m/s,  $\omega$  is the angular frequency (radian per second) and  $\eta = 1.85 \times 10^{-5}$  Pa s, is

the viscosity of air. The impedance of the air cavity, i.e.  $Z_D$ , is given by

$$Z_D = -j \cot\left(\frac{D\omega}{c}\right) \tag{4}$$

The impedance of air  $\rho c$  has normalized all the impedances in Eq. (1)-(4). Therefore, the total acoustic impedance is

$$Z_{total} = Z_{MPP} + Z_D \tag{5}$$

### 2.2 Parallel-Arranged Inhomogeneous Microperforated Panel (iMPP) Absorber

By arranging four inhomogeneous MPP sub-parts to form a single-layer parallel-arranged inhomogeneous microperforated panel (here we denoted such arrangement as iMPP) absorber, such MPP absorber's sound absorption performance can be improved, especially towards the low-frequency region with a broader bandwidth. A similarly arranged squared-shaped MPP model is suggested in the current study, where MPP is provided with four sub-parts of inhomogeneous perforation. This configuration is to affiliate the benefits of a single panel layer consisting of four sub-sections extending the absorption bandwidth in the low-frequency region. The panel has four sub-MPPs arranged parallel to each other and having a different perforation diameter and perforation ratio to generate an inhomogeneous pattern, as shown in Fig. 1b. For the four parallel-arranged iMPP absorbers, this paper discusses three different situations for the back-air cavity between them:

- (i) The parallel-arranged iMPP with a partitioned back cavity. Each sub-MPP has its own separate back cavity.
- (ii) The parallel-arranged iMPP with the partition but with the same back-cavity depth. Each sub-MPP has the same back-cavity depth with partition as of other sub-sections.
- (iii) The parallel-arranged iMPP with the uniform back cavity. Each sub-MPP has the same shared back cavity without partition.

#### 2.2.1 Parallel-Arranged iMPP Absorber with a Partitioned Back Cavity

The complete assembly, including the cavity frame for such a particular arrangement, is shown in Fig. 1a, b, consisting of four sub-MPP arranged parallel with a partitioned back cavity. Figure 1c shows an iMPP absorber considered a parallel combination of four RLC branches based on the electrical equivalent circuit model (ECM). Furthermore, to

avoid contact among the sub-iMPP resonators, the back-air cavity is split into four sub-cavities. So, the normalized acoustic impedance for each sub-iMPP absorber ( $Z_{iMPPsub_i}$ ) is denoted as

$$Z_{iMPPsub_i} = r_{sub_i} + j\omega m_{sub_i} - j \cot\left(\frac{D_i\omega}{c}\right) \tag{6}$$

For each sub-iMPP, the impedance of the back-air cavity, i.e.  $Z_{D_i}$ , is denoted as

$$Z_{D_i} = -j \cot\left(\frac{D_i\omega}{c}\right) \tag{7}$$

$$r_{sub_i} = \frac{32\eta t_i}{p_i \rho c d_i^2} k_{r_i} \tag{8}$$

$$m_{sub_i} = \frac{t_i}{p_i c} k_{m_i}, \tag{9}$$

where

$$k_{r_i} = \sqrt{1 + \frac{k_i^2}{32} + \frac{\sqrt{2}}{32} k_i \frac{d_i}{t_i}} \tag{10}$$

$$k_{m_i} = \left(1 + \left(9 + \frac{k_i^2}{2}\right)^{-1/2} + \frac{0.85d_i}{t_i}\right) \tag{11}$$

The sub-sections of iMPP are denoted as,  $iMPP_{sub_1}$ ,  $iMPP_{sub_2}$ ,  $iMPP_{sub_3}$  and  $iMPP_{sub_4}$ . The specific acoustic impedance of the parallel-arranged iMPP with each relative back cavity, hence, comprises of

$$Z_1 = Z_{iMPPsub_1} + Z_{D_1} \tag{12}$$

$$Z_2 = Z_{iMPPsub_2} + Z_{D_2} \tag{13}$$

$$Z_3 = Z_{iMPPsub_3} + Z_{D_3} \tag{14}$$

$$Z_4 = Z_{iMPPsub_4} + Z_{D_4} \tag{15}$$

Also, for a four parallel-arranged iMPP, the overall acoustic impedance can be expressed as

$$Z_{total} = \left(\sum_{i=1}^4 \frac{a_i}{z_i}\right)^{-1} \tag{16}$$

where  $i = 1, 2, 3, 4$  represents the number of the sub-MPP,  $p_i$  is the perforation ratio of each sub-iMPP,  $t_i$  is the thickness of each sub-iMPP,  $r_i$  and  $m_i$  normalized acoustic resistance reactance of sub-iMPP, respectively,  $D_i$  is the back-cavity

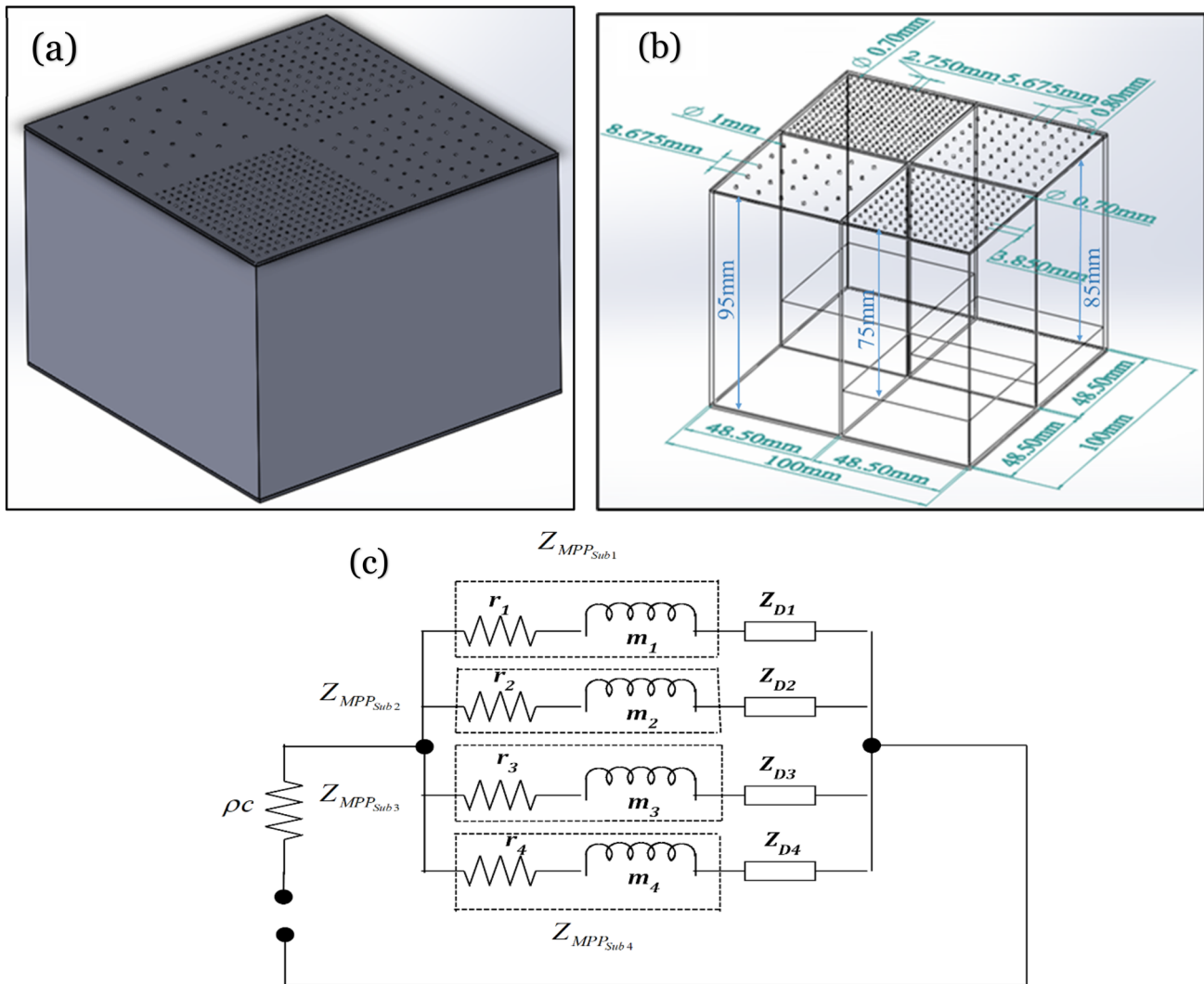


**Fig. 1** Structure of single-layer parallel-arranged iMPP with partitioned cavity: **a** final Model of iMPP, **b** isometric view of model with complete dimensions, **c** the equivalent electrical model

depth of each sub-iMPP. And  $a_i = A_i/A_T$  is the ratio of  $A_i$ =area of the sub-iMPP and  $A_T$ =whole area of the iMPP. The sound absorption coefficient for the normal-incidence state is determined by

$$\alpha = \frac{4Re\{Z_{total}\}}{[1 + Re\{Z_{total}\}]^2 + [Im\{Z_{total}\}]^2} \tag{17}$$

**2.2.2 Parallel-arranged iMPP Absorber with a Partitioned Same Back Cavity**

In this model, each sub-part of parallel-arranged iMPP has the same back-cavity depth, but with partition. The only significant difference between such arrangement and the previous one is that the arrangement, in this case, has the

same-cavity depth at the back of each sub-section of iMPP. The complete structure assembly, including the cavity frame of such arrangement, is shown in Fig. 2a, b, and ECM for this case is also similar as in Fig. 1c. The impedance of the air cavity, i.e.  $Z_{D_i}$ , for such a parallel-arranged iMPP absorber, can be obtained from Eq. (7). Also, the specific acoustic impedance for each sub-iMPP can be obtained from Eq. (6). Similarly, the normalized sound absorption coefficient for such iMPP absorber arrangement can be obtained from Eq. (17).

**2.2.3 Parallel-Arranged iMPP Absorber Without Partition but a Uniform Back Cavity**

In this model, each sub-section of parallel-arranged iMPP shared the uniform back-cavity depth without any partition.

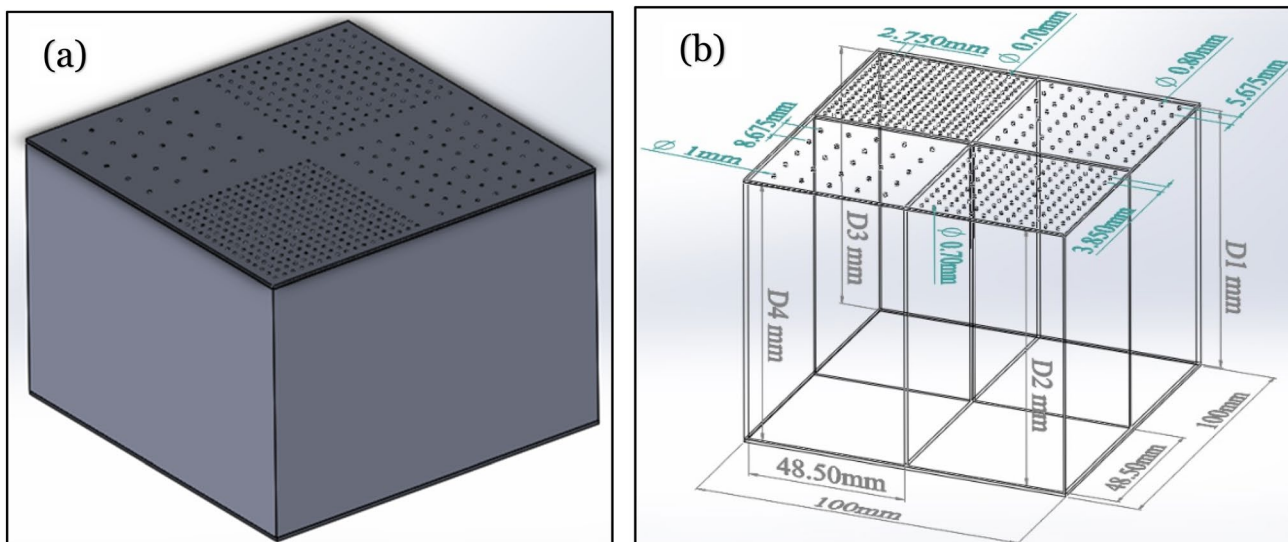


**Fig. 2** Structure of parallel-arranged iMPP without partition cavity **a** final Model of iMPP **b** isometric view of model with complete dimensions

Complete assembly, including the cavity frame, is shown in Fig. 3a, b. The ECM for such an arrangement is shown in Fig. 3c. So, the impedance of air cavity, i.e.  $Z_D$ , for such parallel-arranged inhomogeneous microperforated panel absorber can be obtained from Eq. (4). The specific acoustic impedance for each sub-iMPP is

$$\frac{1}{Z_{iMPP}} = \frac{1}{Z_{iMPP_{sub_1}}} + \frac{1}{Z_{iMPP_{sub_2}}} + \frac{1}{Z_{iMPP_{sub_3}}} + \frac{1}{Z_{iMPP_{sub_4}}} \quad (18)$$

For each sub-MPP absorber, the normalized acoustic impedance is denoted as

$$Z_{iMPP_{sub_i}} = r_i + j\omega m_i \quad (19)$$

For this kind of parallel-arranged iMPP absorber, the total acoustic impedance is expressed as;

$$Z_{total} = Z_{iMPP} + Z_D \quad (20)$$

The normalized sound absorption coefficient for such iMPP absorber arrangement can be obtained from Eq. (17).

### 3 Parametric Study and Simulation Results

#### 3.1 Effects of Inhomogeneous Pattern

The idea of introducing a four parallel-arranged iMPP system is to achieve wider absorption bandwidth in the low-frequency region. In this paper, four different parallel-arranged iMPPs of different impedances are designed; each section has a different hole diameter, perforation

ratio, and a backed air cavity. The inhomogeneous pattern produces mixed acoustic impedance on the surface of the iMPP system. Therefore, the incident sound distinguishes that the iMPP system has four independent acoustic resonators with dissimilar resonant frequencies.

A study is conducted to compare the effectiveness of parallel-arranged iMPP (with partition) against homogeneous MPPs with the same uniform back-cavity depth. Figure 4 presents the results of the sound absorption coefficient of three different single homogeneous MPPs and a parallel-arranged iMPP combined from four different single iMPPs with varying sizes of diameter, perforation ratio, and uniform back-cavity depth with partition. Tables 1 and 2 listed all the single homogeneous MPPs parameters, double homogeneous MPPs, and parallel-arranged iMPPs used for this particular study. From the results in Fig. 4a–d, it can be seen clearly that the combination of multiple sub-cavities in parallel-arranged iMPP shows better frequency bandwidth (185–390 Hz) and a decent average absorption amplitude ( $\alpha = 0.94$ ) compared with different homogeneous MPPs. In Fig. 4a–d, four different back-air cavity depths of 95 mm, 85 mm, 75 mm, and 50 mm are being used. Parallel-arranged iMPP (uniform back cavity with partition) in Fig. 4a with back-air cavity depth of 95 mm shows good results towards the low-frequency region with wider bandwidth and descent amplitude as compared with other back-cavity depths. Also, from Fig. 4b–d, a similar trend can be seen. This illustrates that among different homogeneous MPPs, the four parallel-arranged iMPP (partitioned uniform back-air cavity) shows improved and favourable results. Another point can be seen that as we decrease the cavity depths behind MPP, the absorption peaks shift towards higher

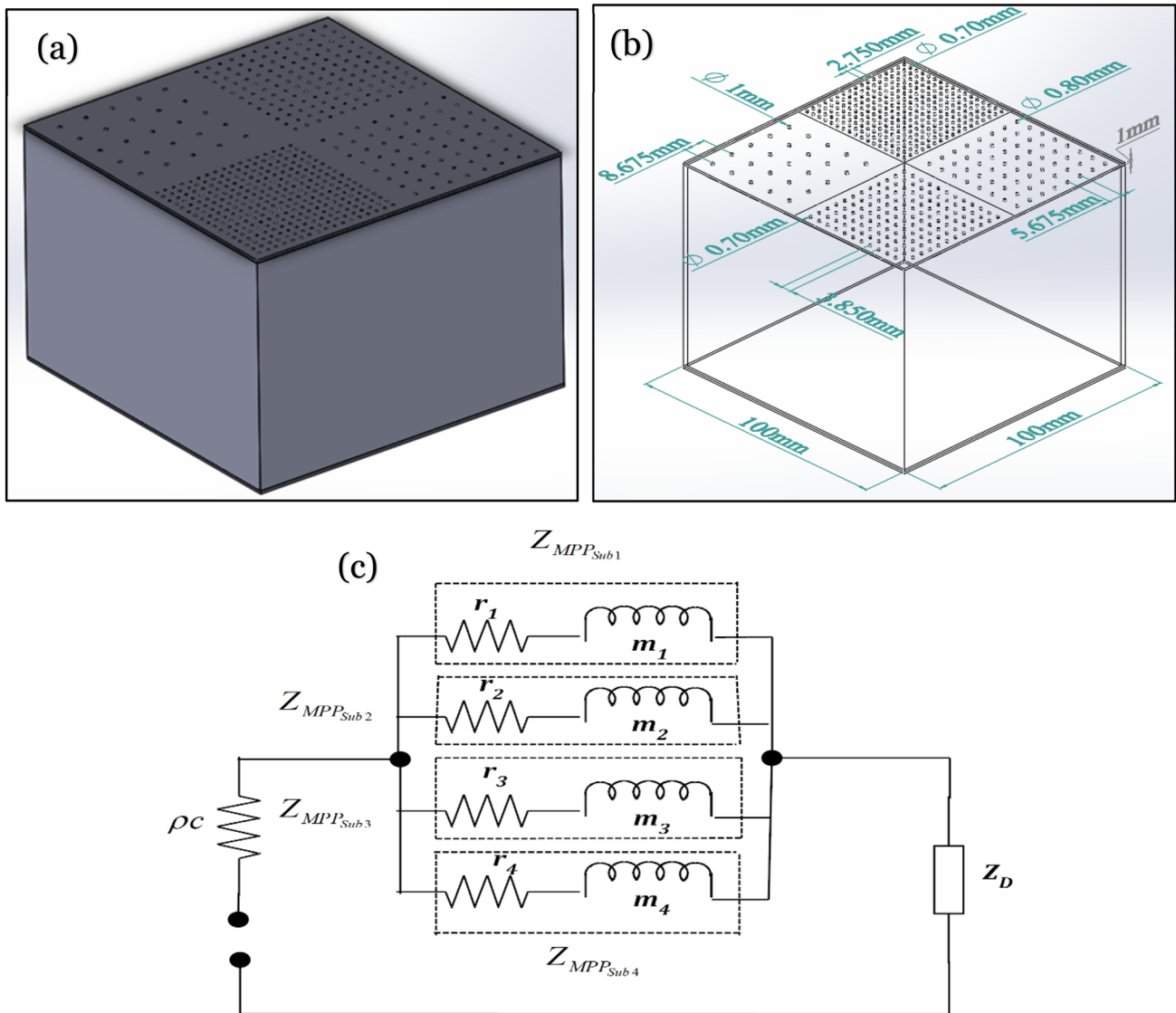


**Fig. 3** Structure of single-layer parallel-arranged iMPP without partition and uniform cavity **a** final model of iMPP, **b** isometric view of model with complete dimensions, **c** the equivalent electrical model

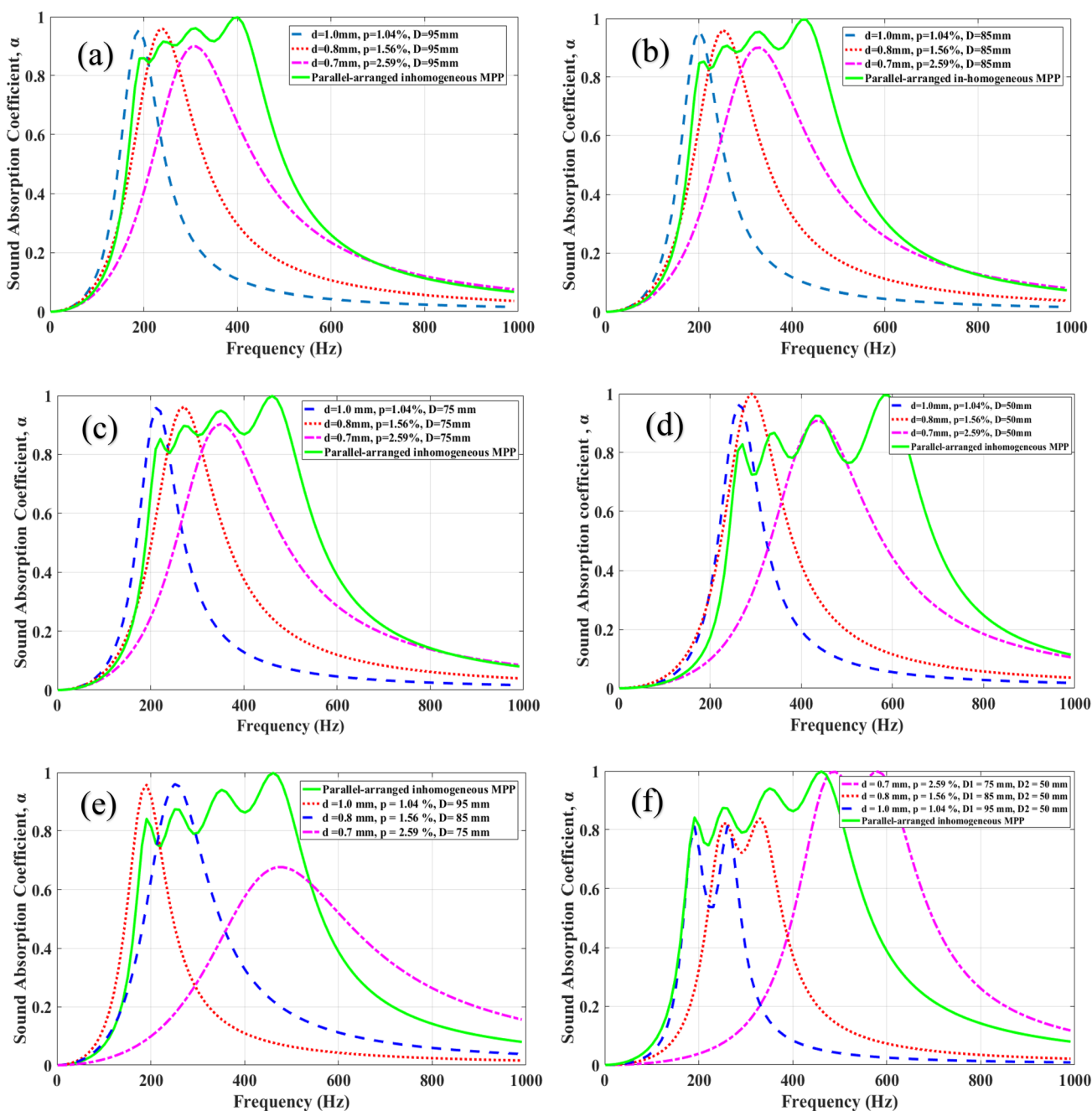
frequency with their amplitude decreasing. The effect of cavity depth has been discussed in detail in Sect. 3.4.

Figure 4e compares the four parallel-arranged iMPP systems' absorption coefficients. Each section has different perforation sizes and different sub-cavity depths with the different homogeneous MPP with the same perforation size and back-cavity depth. Table 2 listed parameters used for the effect of inhomogeneous patterns for such cases. From the results, it can be understood that the absorption bandwidth of four parallel-arranged iMPP is in the lower-frequency region and appreciably wider bandwidth of 195–455 Hz with an average absorption amplitude of  $\alpha = 0.91$  than the other MPPs with homogeneous perforation. A similar trend can be seen in Fig. 4f, here, the comparison of the absorption coefficient for the parallel-arranged iMPP system with

each section having different perforation sizes and different back-cavity depths with that of different homogeneous MPP with the same perforation size but different partitioned back-cavity depths has been carried out. Results show a better and wider frequency bandwidth of 195–455 Hz and a decent average absorption amplitude of  $\alpha = 0.91$  compared with the homogeneous MPPs.

### 3.2 Effects of Perforation Ratio $p$

Another study is conducted to observe the absorption behaviour of parallel-arranged iMPP absorber with different perforation ratios. Hence, a simulation is carried out for the situation where the perforation ratios are dissimilar for each sub-iMPP. The selected perforation ratio determines the



**Fig. 4** Comparison of absorption coefficient of: parallel-arranged iMPP (uniform back cavity) with homogeneous MPPs (uniform back cavity): **a**  $D=95$  mm, **b**  $D=85$  mm, **c**  $D=75$  mm, **d**  $D=50$  mm e

parallel-arranged iMPP (multi-cavity) with homogeneous MPP (single cavity) and **f** parallel-arranged iMPP (multi-cavity) with homogeneous MPP (multi-cavity)

resonant frequency (peak frequency) of the corresponding sub-MPP. By keeping the perforation ratio of one sub-iMPP constant and changing for other sub-iMPPs, the effect of perforation on sound absorption performance is simulated. For four sub-sections of parallel-arranged iMPP different perforations were used and are listed in Table 1. Figure 5a have one fixed, i.e.  $p_1=1.56\%$ , perforation ratio while other three sub-sections have variations. Similarly, Fig. 5b–d have

a similar trend (one fixed perforation ratio sub-section but variation in others).

From Fig. 5a results, when  $p_1=1.56\%$  is fixed and  $p_2=2.59\%$ ,  $p_3=5.08\%$  and  $p_4=1.04\%$ , varied, the average absorption amplitude ( $\alpha=0.94$ ) and frequency bandwidth (185–390 Hz) is the best one. A similar trend can be observed while fixing  $p_2$ ,  $p_3$  and  $p_4$  while changing others, respectively. From the results of Fig. 5, it can be observed

**Table 1** Parameters for the comparison between different single-layer homogeneous MPPs with four parallel-arranged iMPP (Uniform back-cavity depth with partition)

Sample	Hole diameter (mm)				Thickness $t$ (mm)	$p_1$ (%)	$p_2$ (%)	$p_3$ (%)	$p_4$ (%)
	$d_1$	$d_2$	$d_3$	$d_4$					
<i>D = 95 mm</i>									
MPP1	1.00				1.0	1.04			
MPP2	0.80				1.0	1.56			
MPP3	0.70				1.0	2.59			
i-MPP	0.80	0.70	0.70	1.00	1.0	1.56	2.59	5.08	1.04
<i>D = 85 mm</i>									
MPP1	1.00				1.0	1.04			
MPP2	0.80				1.0	1.56			
MPP3	0.70				1.0	2.59			
i-MPP	0.80	0.70	0.70	1.00	1.0	1.56	2.59	5.08	1.04
<i>D = 75 mm</i>									
MPP1	1.00				1.0	1.04			
MPP2	0.80				1.0	1.56			
MPP3	0.70				1.0	2.59			
i-MPP	0.80	0.70	0.70	1.00	1.0	1.56	2.59	5.08	1.04
<i>D = 50 mm</i>									
MPP1	1.00				1.0	1.04			
MPP2	0.80				1.0	1.56			
MPP3	0.70				1.0	2.59			
i-MPP	0.80	0.70	0.70	1.00	1.0	1.56	2.59	5.08	1.04

**Table 2** Parameters for the comparison between different single-layer homogeneous MPPs with parallel-arranged iMPP (Multi-cavity depth)

Sample	Hole diameter				Thickness $t$ (mm)	$p_1$ (%)	$p_2$ (%)	$p_3$ (%)	$p_4$ (%)	$D_1$ (mm)	$D_2$ (mm)	$D_3$ (mm)	$D_4$ (mm)
	$d_1$ (mm)	$d_2$ (mm)	$d_3$ (mm)	$d_4$ (mm)									
MPP1	1.00				1.0	1.04				95			
MPP2	0.80				1.0	1.56				85			
MPP3	0.70				1.0	2.59				75			
i-MPP	0.80	0.70	0.70	1.00	1.0	1.56	2.59	5.08	1.04	85	75	75	95
MPP1	1.00				1.0	1.04				95	50		
MPP2	0.80				1.0	1.56				85	50		
MPP3	0.70				1.0	2.59				75	50		
i-MPP	0.80	0.70	0.70	1.00	1.0	1.56	2.59	5.08	1.04	85	75	75	95

clearly that by reducing the perforation ratio, the resonance frequency shifts towards a lower frequency, thus reducing the amplitude of the absorption coefficient. Similarly, by increasing the perforation ratio of sub-iMPP, the amplitude of the lower resonance frequency increases and moves to the higher frequency close to resonance.

### 3.3 Effects of Hole Diameter $d$

In this case, the simulation was performed with MATLAB software on a single-layer parallel-arranged iMPP1 ( $d_1=0.8$  mm,  $d_2=0.7$  mm,  $d_3=0.7$  mm,  $d_4=1.0$  m) with  $D_1=85$  mm,  $D_2=75$  mm,  $D_3=75$  mm,  $D_4=95$  mm, respectively. By keeping the diameter of the holes for one

sub-iMPP, i.e.  $d_1$ , fixed and the diameter of the other sub-iMPP, i.e.  $d_2$ ,  $d_3$  and  $d_4$  is varied. The perforation ratios for the sub-iMPPs of four parallel-arranged iMPP are  $p_1=1.56\%$ ,  $p_2=2.59\%$ ,  $p_3=5.08\%$  and  $p_4=1.04\%$ , respectively. Table 3, listed parameters used for this particular study.

Figure 6a shows the results when  $d_1=0.8$  mm ( $p_1=1.56\%$ ) is fixed and  $d_2$ ,  $d_3$  and  $d_4$  ( $p_2=2.59\%$ ,  $p_3=5.08\%$  and  $p_4=1.04\%$ ) is varied. For  $d_1=0.8$  mm,  $d_2=0.7$  mm,  $d_3=0.7$  mm,  $d_4=1.0$  mm, the absorption peak ( $\alpha=1.02$ , 455 Hz) and the frequency bandwidth of 185 Hz–455 Hz are the best among others. But as the diameter of other sub-iMPPs decreases, the absorption peak of  $\alpha=0.92$  at 240 Hz and a frequency bandwidth of 135–245 Hz is the least



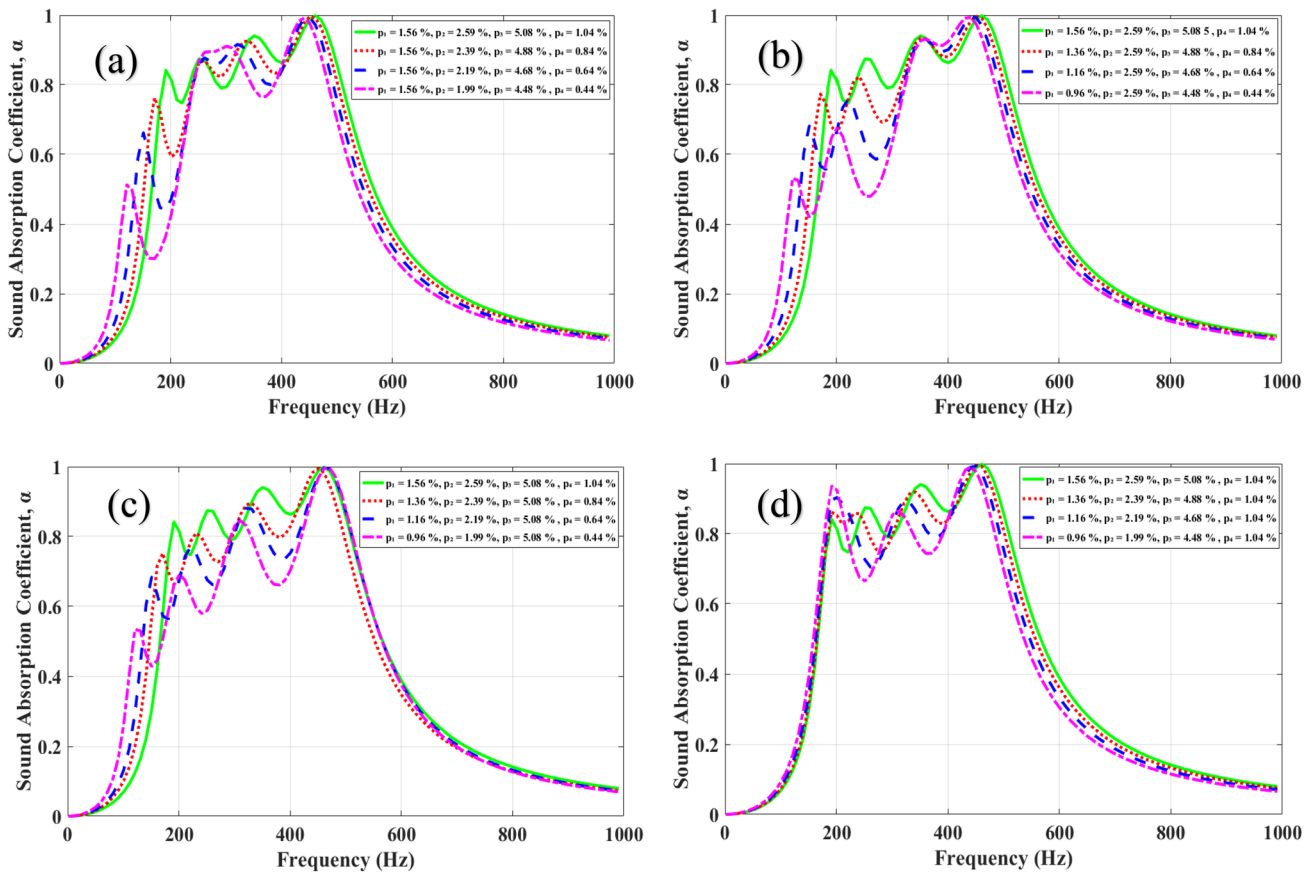


**Fig. 5** Effect of perforation ratio on absorption coefficient of the single-layer four parallel-arranged iMPP:  $d_1=0.8$  mm,  $d_2=0.7$  mm,  $d_3=0.7$  mm,  $d_4=1.0$  mm,  $t=1$  mm **a**  $p_1=1.56\%$  fixed, others varies,

**b**  $p_2=2.59\%$  fixed, others varies, **c**  $p_3=5.08\%$  fixed, others varies, **d**  $p_4=1.04\%$  fixed, others varies

among all. From the results, it has been observed that as the diameter  $d_2, d_3$  and  $d_4$  is reduced, the frequency bandwidth and absorption coefficient decrease. However, reducing the diameter of sub-iMPP with a higher perforation rate can significantly improve absorption coefficient and bandwidth compared with sub-iMPP, with a large diameter and smaller perforation ratio. A similar trend can be seen in Fig. 6b–d by fixing  $d_2=0.7$  mm,  $d_3=0.7$  mm,  $d_4=1.0$  mm, and varying others, respectively. Overall, from the results in Fig. 6, by decreasing hole diameter with greater perforation ratio, the absorption peak at the lower resonance frequency increases, and frequency bandgap widens compared to increasing hole diameter with a smaller perforation ratio (Table 3).

### 3.4 Effect of Backed Cavity Depth D

In this case, four different arrangements (iMPP1, iMPP2, iMPP3, iMPP4) of the single-layer four parallel-arranged iMPP with back-air cavity partitioned into four sub-cavities of the same depths have been used. Figure 7 shows the effect of the combination of the backed cavity depths for the

single-layer parallel-arranged iMPP. Table 4 includes all the parameters used in the MATLAB study for four different arrangements of iMPP. Figure 7a present the results of a single layer of four parallel-arranged iMPP1 ( $d_1=0.8$  mm,  $d_2=0.7$  mm,  $d_3=0.7$  mm,  $d_4=1.0$  m) with a back-air cavity of  $D_1-D_4=95, 85, 75,$  and  $50$  mm used, respectively. Results show that as we increase the back-cavity depth, the absorption peak moves towards the lower-frequency region and vice versa. With the back-cavity of the depth of 95 mm, the best absorption bandwidth of 185–395 Hz has been observed with an average absorption of more than 90% ( $\alpha = 0.94$ ). Similar trend can be seen for iMPP2 ( $d_1=1.0$  mm,  $d_2=0.7$  mm,  $d_3=0.8$  mm,  $d_4=0.7$  mm) in Fig. 7b iMPP3 ( $d_1=1.0$  mm,  $d_2=0.8$  mm,  $d_3=0.7$  mm,  $d_4=0.7$  mm) in Fig. 7c and iMPP4 ( $d_1=1.0$  mm,  $d_2=0.7$  mm,  $d_3=0.7$  mm,  $d_4=0.8$  mm) in Fig. 7d, respectively.

Figure 8 shows the results for a single layer of four parallel-arranged iMPP1 with each sub-iMPP1 having uniform back-cavity depth with partition. From Fig. 8a, here, the cavity depth ( $D_1=85$  mm) of one sub-iMPP1 remains constant while other sub-cavities ( $D_2, D_3, D_4$ ) are varied. When the

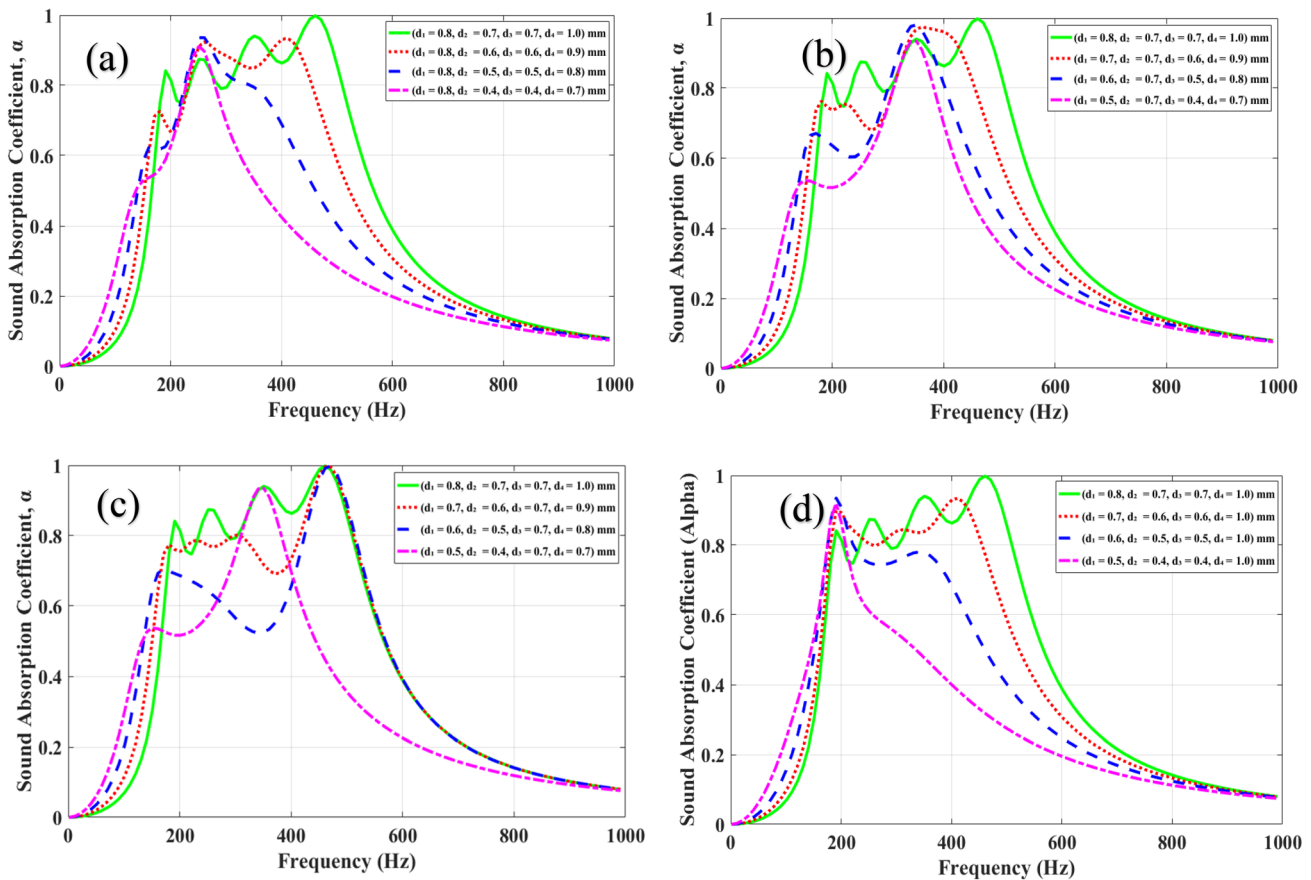


**Fig. 6** Effect of hole diameter on the sound absorption coefficient of the parallel-arranged iMPP **a**  $d_1=0.8$  mm fixed, others varied **b**  $d_2=0.7$  mm fixed, others varied **c**  $d_3=0.7$  mm fixed, others varied **d**  $d_4=1.0$  mm fixed, others varied

cavity depth is of the same value, i.e. 85 mm, behind all sub-MPPs, it shows an average absorption coefficient of more than 90% ( $\alpha = 0.93$ ) with wider bandwidth of 195–425 Hz is best among other sub-cavities. Results show that as the back-cavity depth increases, the absorption peaks move towards the low-frequency region. However, the opposite behaviour has been observed as the back-cavity depth decreases, the absorption peak moves towards a higher frequency.

Figure 8b shows the results when the same sub-iMPP1 back cavity ( $D_1$ ) is now varied, but the other sub-iMPP1 cavities ( $D_2, D_3, D_4 = 85$  mm) remained fixed. It can be seen clearly that due to variation in the first sub-cavity depth, the first peak in lower frequency shows a fluctuating behaviour, which indicates that as the sub-iMPP1 back cavity ( $D_1$ ) decreases, the peak in lower frequency also decreases and shrinking the bandwidth. Similar behaviour has been observed for the other cases as in Fig. 9a  $D_2 = 75$  mm, fixed and  $D_1, D_3, D_4$  varied and in Fig. 9b  $D_2$  varied and  $D_2, D_3, D_4$  is fixed (75 mm), Fig. 10a  $D_3 = 75$  mm, Fixed and  $D_1, D_2, D_4$  is varied, Fig. 10b  $D_3$  varied and  $D_1, D_2, D_4$  is fixed (75 mm), Fig. 11a  $D_4 = 95$  mm, Fixed and  $D_1, D_2, D_3$  is varied, Fig. 11b  $D_4$  varied and  $D_1, D_2, D_3$  fixed (95 mm).

Overall, this study has observed that fixing one of the cavities and varying others makes absorption peaks show fluctuations and alter the bandwidth. With increased cavity depth, the absorption peaks move towards the lower-frequency region with improved bandwidth. Similarly, decreasing the cavity depth makes absorption peaks shift towards higher frequency regions with expanding bandwidths, which is no obligation of this current study.

### 3.5 Effect of Back-Cavity width $W$

Another parametric study analysis is performed on the mathematical model in MATLAB software, and iMPP1 has been chosen for this study. Different parameters of iMPP1 have been listed in Table 5. Figure 12 shows the effect of using different widths but with the same back-air cavity depth on absorption coefficient under different parallel-arranged sub-sections of inhomogeneous MPP1. The arrangement of the sub-section of iMPP1 used here is also shown in Fig. 14.

In Fig. 12 a the width of sub-Sect. 1 and 2 is fixed, i.e.  $W_{1,2} = 50$  mm but for 3 and 4 is varying, i.e.  $W_{3,4} = (50-50, 60-40, 70-30$  and  $80-20)$  mm, respectively. The effect of

**Table 3** Parameters used for the effect of diameter on parallel-arranged iMPP (Multi-cavity depth)

Sample	Hole diameter (mm)			Thickness t (mm)	$p_1$ (%)	$p_2$ (%)	$p_3$ (%)	$p_4$ (%)
	$d_2$	$d_3$	$d_4$					
$d_1=0.8(\text{mm})$ , fixed								
MPP1	0.70	0.70	1.00	1.0	1.56	2.59	5.08	1.04
	0.60	0.60	0.90	1.0	1.56	2.59	5.08	1.04
	0.50	0.50	0.80	1.0	1.56	2.59	5.08	1.04
	0.40	0.40	0.70	1.0	1.56	2.59	5.08	1.04
$d_2=0.7(\text{mm})$ , fixed								
MPP1	0.80	0.70	1.00	1.0	1.56	2.59	5.08	1.04
	0.70	0.60	0.90	1.0	1.56	2.59	5.08	1.04
	0.60	0.50	0.80	1.0	1.56	2.59	5.08	1.04
	0.50	0.40	0.70	1.0	1.56	2.59	5.08	1.04
$d_3=0.7(\text{mm})$ , fixed								
MPP1	0.80	0.70	1.00	1.0	1.56	2.59	5.08	1.04
	0.70	0.60	0.90	1.0	1.56	2.59	5.08	1.04
	0.60	0.50	0.80	1.0	1.56	2.59	5.08	1.04
	0.50	0.40	0.70	1.0	1.56	2.59	5.08	1.04
$d_4=1.0(\text{mm})$ , fixed								
MPP1	0.80	0.70	0.70	1.0	1.56	2.59	5.08	1.04
	0.70	0.60	0.60	1.0	1.56	2.59	5.08	1.04
	0.60	0.50	0.50	1.0	1.56	2.59	5.08	1.04
	0.50	0.40	0.40	1.0	1.56	2.59	5.08	1.04

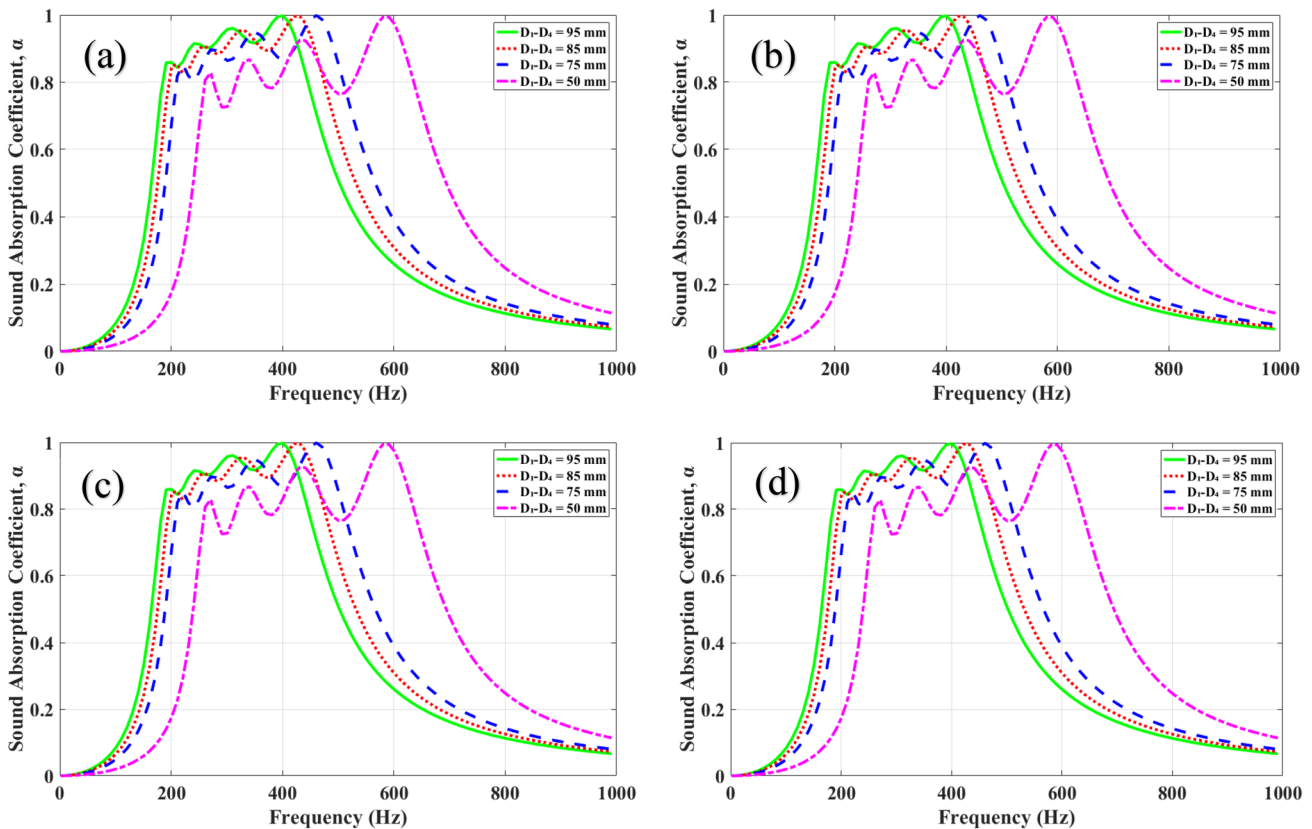


**Fig. 7** Effect of cavity depth on absorption coefficient of parallel-arranged iMPPs **a** MPP1:  $d_1=0.8$  mm,  $d_2=0.7$  mm,  $d_3=0.7$  mm,  $d_4=1.0$  mm, **b** MPP2:  $d_1=1.0$  mm,  $d_2=0.7$  mm,  $d_3=0.8$  mm,

$d_4=0.7$  mm, **c** MPP3,  $d_1=1.0$  mm,  $d_2=0.8$  mm,  $d_3=0.7$  mm,  $d_4=0.7$  mm, **d**  $d_1=1.0$  mm,  $d_2=0.7$  mm,  $d_3=0.7$  mm,  $d_4=0.8$  mm ( same-cavity depth under different sub-sections)

**Table 4** Parameters used for the effect of different cavity depth on Parallel-arranged iMPP (same-cavity depth)

Sample	Hole diameter (mm)				Thickness <i>t</i> (mm)	$p_1$ (%)	$p_2$ (%)	$p_3$ (%)	$p_4$ (%)
	$d_1$	$d_2$	$d_3$	$d_4$					
<b><math>D_1-D_4=95</math> mm</b>									
iMPP1	0.80	0.70	0.70	1.00	1.0	1.56	2.59	5.08	1.04
iMPP2	1.00	0.70	0.80	0.70	1.0	1.04	2.59	1.56	5.08
iMPP3	1.00	0.80	0.70	0.70	1.0	1.04	1.56	2.59	5.08
iMPP4	1.00	0.70	0.70	0.80	1.0	1.04	2.59	5.08	1.56
<b><math>D_1-D_4=85</math> mm</b>									
iMPP1	0.80	0.70	0.70	1.00	1.0	1.56	2.59	5.08	1.04
iMPP2	1.00	0.70	0.80	0.70	1.0	1.04	2.59	1.56	5.08
iMPP3	1.00	0.80	0.70	0.70	1.0	1.04	1.56	2.59	5.08
iMPP4	1.00	0.70	0.70	0.80	1.0	1.04	2.59	5.08	1.56
<b><math>D_1-D_4=75</math> mm</b>									
iMPP1	0.80	0.70	0.70	1.00	1.0	1.56	2.59	5.08	1.04
iMPP2	1.00	0.70	0.80	0.70	1.0	1.04	2.59	1.56	5.08
iMPP3	1.00	0.80	0.70	0.70	1.0	1.04	1.56	2.59	5.08
iMPP4	1.00	0.70	0.70	0.80	1.0	1.04	2.59	5.08	1.56
<b><math>D_1-D_4=50</math> mm</b>									
iMPP1	0.80	0.70	0.70	1.00	1.0	1.56	2.59	5.08	1.04
iMPP2	1.00	0.70	0.80	0.70	1.0	1.04	2.59	1.56	5.08
iMPP3	1.00	0.80	0.70	0.70	1.0	1.04	1.56	2.59	5.08
iMPP4	1.00	0.70	0.70	0.80	1.0	1.04	2.59	5.08	1.56

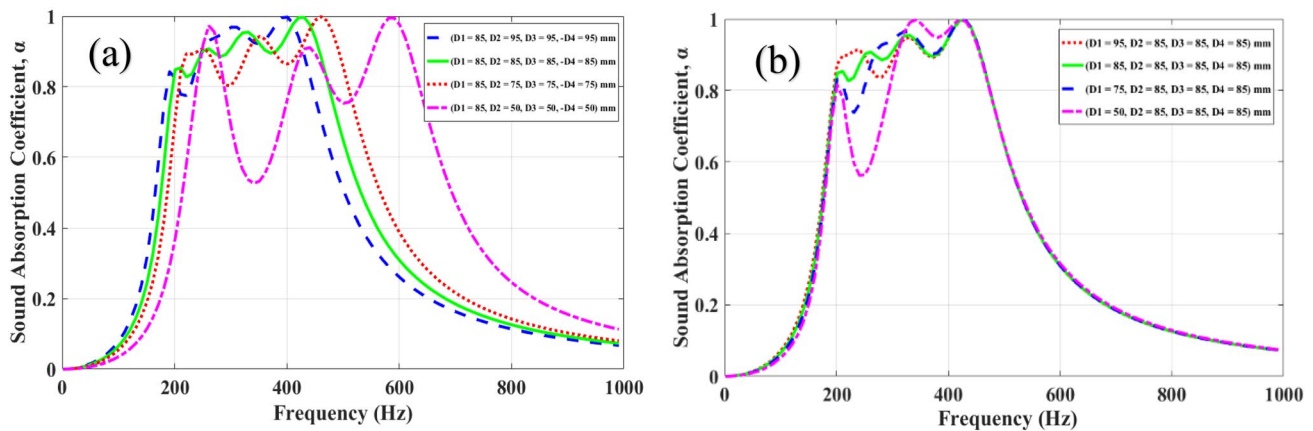
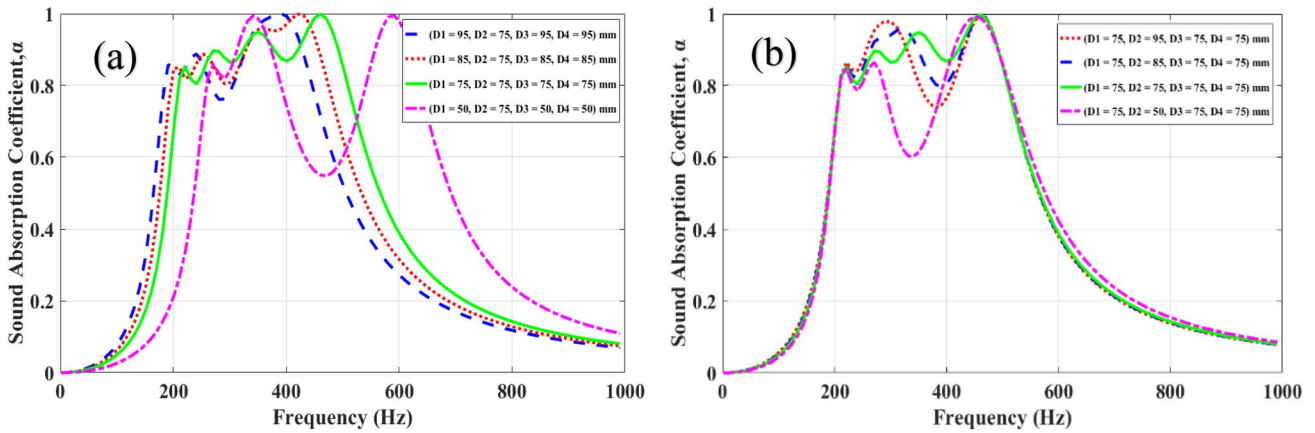


**Fig. 8** Effect of cavity depth on sound absorption coefficient of the parallel-arranged iMPP:  $d_1=0.8$  mm,  $d_2=0.7$  mm,  $d_3=0.7$  mm,  $d_4=1.0$  mm,  $p_1=1.56\%$ ,  $p_2=2.59\%$ ,  $p_3=5.08\%$ ,  $p_4=1.04\%$ , **a**  $D_1=85$  mm, Fixed and  $D_2, D_3, D_4$  varied **b**  $D_1$  varied and  $D_2, D_3, D_4$  fixed

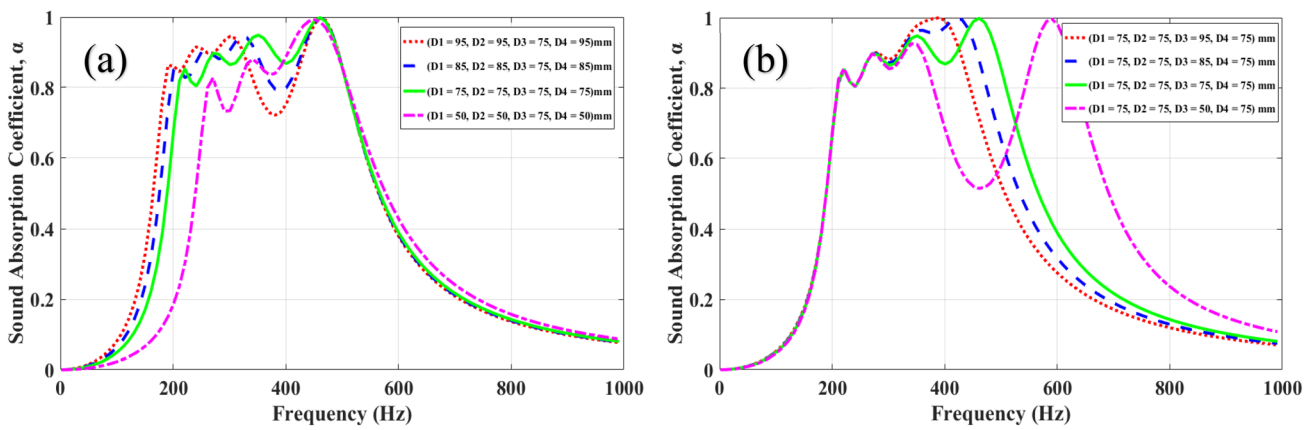
variation in widths of sub-Sect. 3 and 4 on the absorption coefficient can be easily seen and observed in the curves of Fig. 12. The peaks of absorption curves show declined behaviour as we vary the width of sub-Sect. 3 and 4, which results in an overall reduction in average absorption coefficient performance. However, the absorption bandwidth is not much affected. Also, in Fig. 12b, when the sub-Sects. 3 and 4 are now remained fixed, i.e.  $W_{3,4}=50$  mm, however, the sub-Sect. 1 and 2, the width is now varying, i.e.  $W_{1,2}=(50-50, 60-40, 70-30$  and  $80-20)$  mm, respectively,

similar behaviour has been observed. The overall average sound absorption decreases with variation in sub-section widths with the same back-air cavity depth of parallel-arranged inhomogeneous MPP.

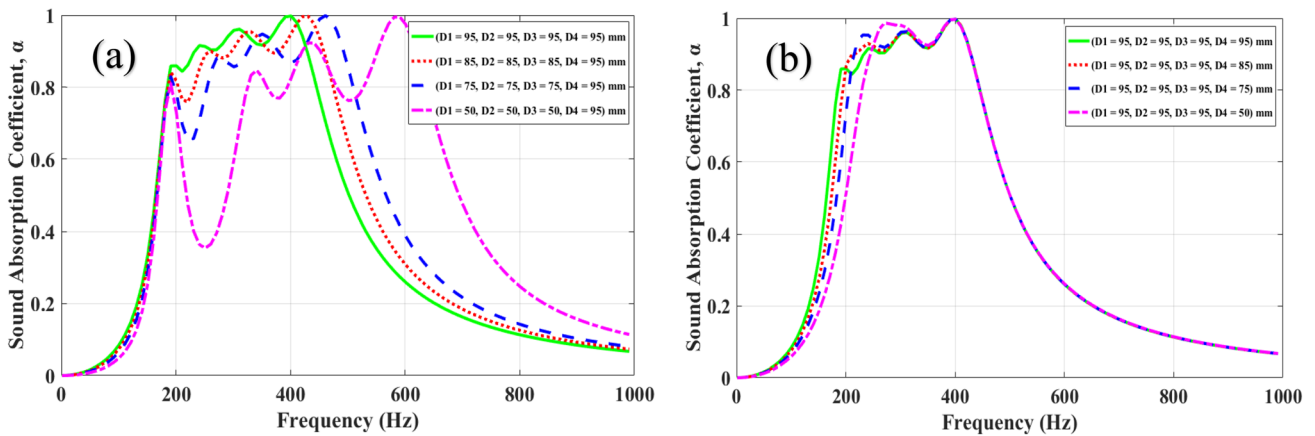
Figure 13 shows the effect of using different widths and different back-air cavity depths on the absorption coefficient under different parallel-arranged sub-sections of inhomogeneous MPP1. In Fig. 13a, the width of sub-Sect. 1 and 2 is fixed, i.e.  $W_{1,2}=50$  mm but for 3 and 4 is varying, i.e.  $W_{3,4}=(50-50, 60-40, 70-30$  and  $80-20)$



**Fig. 9** Effect of cavity depth on sound absorption coefficient of the parallel-arranged iMPP1:  $d_1=0.8$  mm,  $d_2=0.7$  mm,  $d_3=0.7$  mm,  $d_4=1.0$  mm,  $p_1=1.56\%$ ,  $p_2=2.59\%$ ,  $p_3=5.08\%$ ,  $p_4=1.04\%$ , **a**  $D_2=75$  mm, Fixed and  $D_1, D_3, D_4$  varied **b**  $D_2$  varied and  $D_1, D_3, D_4$  fixed



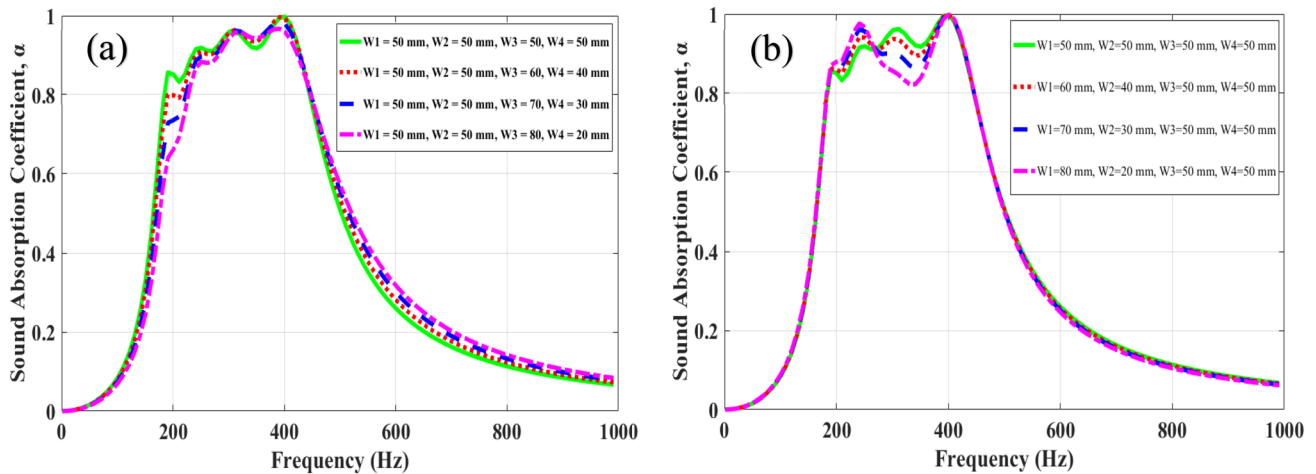
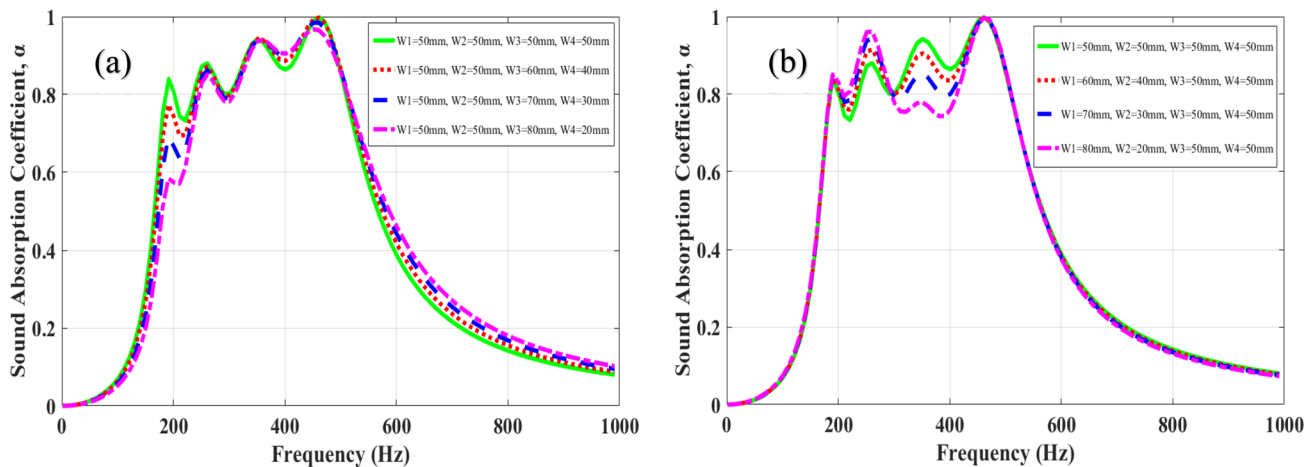
**Fig. 10** Effect of cavity depth on sound absorption coefficient of the parallel-arranged iMPP1:  $d_1=0.8$  mm,  $d_2=0.7$  mm,  $d_3=0.7$  mm,  $d_4=1.0$  mm,  $p_1=1.56\%$ ,  $p_2=2.59\%$ ,  $p_3=5.08\%$ ,  $p_4=1.04\%$ , **a**  $D_3=75$  mm, Fixed and  $D_1, D_2, D_4$  varied **b**  $D_3$  varied and  $D_1, D_2, D_4$  fixed



**Fig. 11** Effect of cavity depth on sound absorption coefficient of the parallel-arranged iMPP1:  $d_1=0.8$  mm,  $d_2=0.7$  mm,  $d_3=0.7$  mm,  $d_4=1.0$  mm,  $p_1=1.56\%$ ,  $p_2=2.59\%$ ,  $p_3=5.08\%$ ,  $p_4=1.04\%$ , **a**  $D_4=95$  mm, Fixed and  $D_1, D_2, D_3$  varied **b**  $D_4=95$  mm, varied and  $D_1, D_2, D_3$  fixed

**Table 5** Parameters used for the effect of different cavity width on parallel-arranged iMPP1 (both same and different cavity depth)

Sample	Hole diameter (mm)				Thickness t (mm)	Perforation ratio 1, $p_1$ (%)	Perforation ratio 2, $p_2$ (%)	Perforation ratio 3, $p_3$ (%)	Perforation ratio 4, $p_4$ (%)	$D_1$ (mm)	$D_2$ (mm)	$D_3$ (mm)	$D_4$ (mm)
	$d_1$	$d_2$	$d_3$	$d_4$									
iMPP1	0.8	0.7	0.7	1.0	1.0	1.04	2.59	5.08	1.04	95	95	95	95
iMPP1	0.8	0.7	0.7	1.0	1.0	1.04	2.59	5.08	1.04	85	75	75	95

**Fig. 12** Effect of variation in widths of sub-sections on the absorption coefficient of parallel-arranged iMPP1 with same back-cavity depths ( $D=95$  mm)**Fig. 13** Effect of variation in widths of sub-sections on absorption coefficient of parallel-arranged iMPP1 with different back-cavity depths ( $D_1=85$  mm,  $D_2=75$  mm,  $D_3=75$  mm,  $D_4=95$  mm)

mm, respectively, with multiple back-air cavity depth of  $D_1=85$  mm,  $D_2=75$  mm,  $D_3=75$  mm and  $D_4=95$  mm, respectively. Under this situation, the first absorption curve shows declined behaviour as we vary the widths of sub-Sect. 3 and 4, which results in a fall of the overall average sound absorption coefficient. However, the absorption bandwidth is not much affected, which shows

the uniqueness of the current designed model of parallel-arranged inhomogeneous MPP. Likewise, in Fig. 13b, when the sub-Sects. 3 and 4 are now remained fixed, i.e.  $W_{3,4}=50$  mm, however in sub-Sect. 1 and 2, the width is now varying, i.e.  $W_{1,2}=(50-50, 60-40, 70-30$  and  $80-20)$  mm, respectively, similar behaviour has been observed as observed earlier. The second and third absorption curves

show declined performance, resulting in a dropping overall average absorption coefficient.

Results show that the overall average sound absorption decreases with variation in sub-section widths with the same back-air cavity depth of parallel-arranged inhomogeneous MPP. Likewise, when using different width and cavity depths the results shows a fall of the overall average sound absorption coefficient. However, the absorption bandwidth is not much affected, which shows the uniqueness of the current designed model of parallel-arranged inhomogeneous MPP (Fig. 14).

#### 4 Finite Element Method (FEM) Simulation

Numerical simulation using FE model in COMSOL Multiphysics 5.5a software has been conducted to study the acoustic performance of SL-iMPP with multi and same back-cavity depth (i.e.  $D=95$  mm, 85 mm, 75 mm, and 50 mm, respectively) with partition. Figure 15 shows the construction of the 3D structure in the FE model that combines the SL-iMPP, which is placed in front of a partitioned air cavity with rigid termination. An adiabatic plane acoustic wavefield is generated by a sound source located at the front boundary to excite the MPP. The SL-iMPP and the backed wall are assumed to be acoustically rigid (no vibration) and isothermal.

The custom meshing of the FE model has been chosen for the simulation to ensure the model produces the valid results of acoustic impedance up to the required frequency. Figure 16 shows the 3D view of the mesh in the FE model. The specific acoustic impedance of the SL-iMPP in the FE model can be obtained by calculating the ratio of the pressure gradient across the panel to the velocity of the fluid across the hole in the direction of propagation. This can be represented as [21]

$$Z_{MPP} = \frac{\int P_i - \int P_t}{\rho c \int v} \quad (21)$$

where  $P_i$  represents the total incident sound pressure at the front surface of the MPP and  $P_t$  is the total transmitted sound pressure at the back surface of the MPP, and  $v$  is the average particle velocity of the fluid. The total impedance of the model is then can be calculated using Eq. 16 and Eq. 17, respectively. The FEM results compared with predicted and experimental results have been shown in Sect. 5.4.

### 5 Experimental Validation

#### 5.1 Materials

Daylight Precision Hard White Resin is the material used to make parallel-arranged DL-iMPP samples. The material produces samples of high strength, precision, exceptional tensile strength (80 MPa), washable, high precision, and

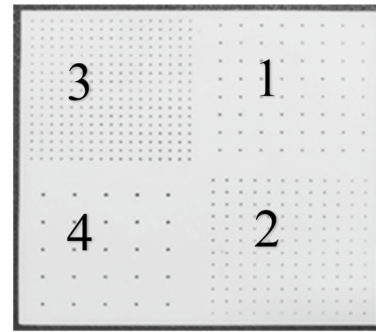


Fig. 14 Arrangement of sub-sections of parallel-arranged inhomogeneous MPP1 (iMPP1) II

elongation comparable to acrylic and polyamide. It has a density of about  $1.09 \text{ g/cm}^3$ .

#### 5.2 Sample Fabrication

For the experiments, four parallel-arranged iMPP samples with different arrangements of sub-sections with different perforations were made using a 3D printing-based Liquid Crystal Display (LCD) technology which is based on Stereolithography with the Youchuang 3D printer, as shown in Fig. 17. The structural parameters of the samples used in the experimental study are listed in Table 6. The cavities behind each sub-section of iMPP were also prepared using the same material with a partition separating the four cavities and rigid mass to modulate each cavity's depth, Fig. 19. The detailed characterization of the 3D printed samples has been done using 3DMeasuring Laser Microscope (Olympus LEXT OLS4000) as shown in Fig. 18 (Fig. 19).

#### 5.3 Experimental Setup and Absorption Coefficient Measurement

Experimental validation is performed on a square impedance tube with two microphones based on the transfer function method and ISO 10534–2 standard [22] for the normal-incidence sound absorption. The impedance tube has a square-shaped inner cross-section with a side length of 100 mm. Two half-inch pre-polarized free-field acoustic microphones (B&K Type 4958-A) with a (B&K Type 3160-A-042) being used in the experiment as shown in Figs. 20 and 21. The signal analyser is used as a data acquisition system to process the recorded pressure signal. Then, the B&K method-based PULSE software installed in the computer calculates the test sample's normal incident acoustic characteristics based on the frequency response function measured between the various measurement positions.

Firstly, the measured sample is held firmly into the square impedance tube, making sure it is completely sealed [23].

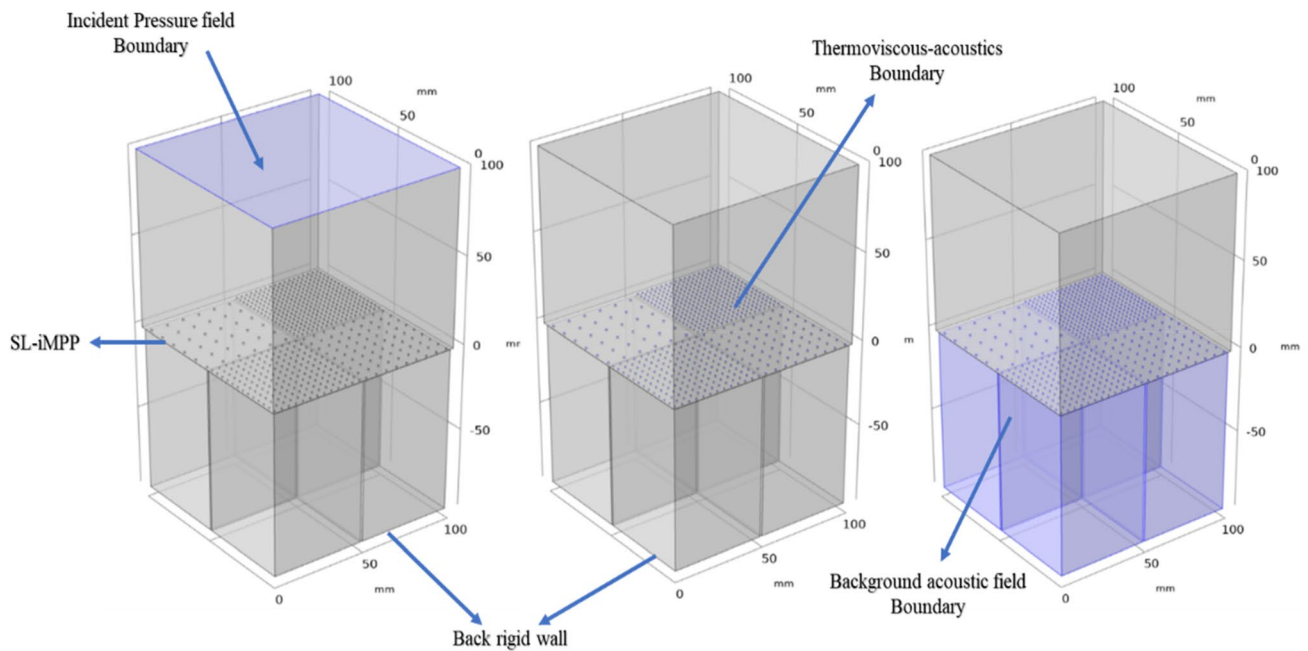


**Fig. 15** Schematic diagram of the 3D FE model of SL-iMPP with different boundary condition in COMSOL 5.5a Multiphysics Software

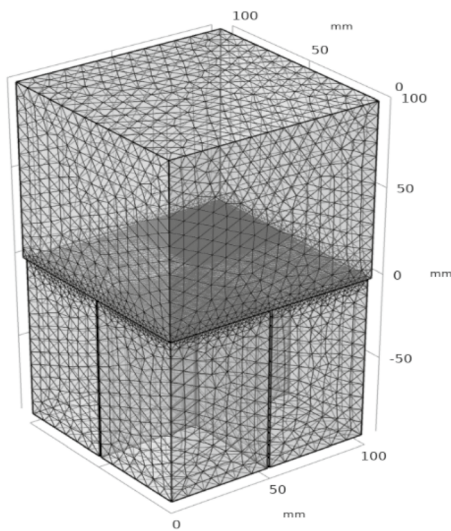


**Fig. 16** The meshing of the 3D FE model of SL-iMPP in COMSOL 5.5a Multiphysics software

The loudspeaker at one end of the tube then emits a precisely quantified sound (10–1000 Hz), while the microphones measure the sound pressure level at a specific location along the length of the tube. The distance between the loudspeaker and the first microphone (Mic 1) is 30 cm, whereas the distance between the two adjacent microphones (Mic 1 and Mic 2) is 10 cm. However, the distance between the second microphone (Mic 2) and the test sample is 10 cm. Experimental measurement was performed on four different samples of parallel-arranged iMPP, listed in Table 6. Each test

is repeated at least three times to ensure the measurement result changes and obtain the average result of the measured absorption coefficient in the low-frequency region with wide bandwidth.

#### 5.4 Experiment Results and Validation

Figure 22 shows the verification of the ECM-based MATLAB predicted and FEM simulation results with measured from experiment results for a single-layer four parallel-arranged iMPPs with partitioned multi-cavity. It can be seen clearly that the theoretical prediction and FEM results agreed reasonably well with the experimentally measured results. Figure 22a shows that the measured experimental data for iMPP1 presents peaks between 195 and 455 Hz with an average absorption coefficient of  $\alpha = 0.84$ . The inconsistency of the measured curve with that of the predicted and FEM curves is due to many reasons: thin structure, inaccuracy of apparatus, sound transmission, and reflection losses during the experiment. Similar behaviour can be observed in Fig. 22b for iMPP2, Fig. 22c for iMPP3, and Fig. 22d for iMPP4. After using four different arrangements of single-layer four parallel-arranged iMPP and their results, the overall pattern of the curves remained the same in predicted, FEM simulation and measured results due to the same overall effect of using different arrangements but with similar parameters. The predicted and FEM curves are slightly higher than measured curves, but the overall trend of the measured results agrees well with anticipated results.



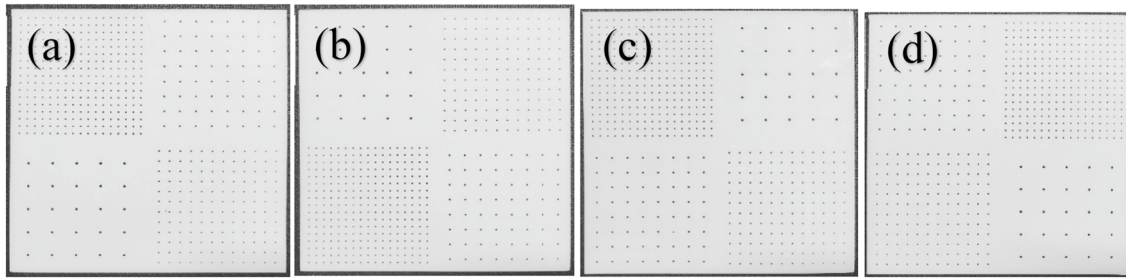


**Fig. 17** Liquid Crystal Display (LCD) technology-based 3D printed samples of the four different arrangements of the parallel-arranged iMPP **a** iMPP1, **b** iMPP2 **c** iMPP3 **d** iMPP4

**Table 6** Parameters used for 3D printing using Liquid Crystal Display (LCD) technology for single-layer parallel-arranged iMPP samples (multi-cavity depth)

Sample	Hole diameter (mm)				Thickness t (mm)	Perforation ratio 1, $p_1$ (%)	Perforation ratio 2, $p_2$ (%)	Perforation ratio 3, $p_3$ (%)	Perforation ratio 4, $p_4$ (%)	$D_1$	$D_2$	$D_3$	$D_4$
	$d_1$	$d_2$	$d_3$	$d_4$									
iMPP1	0.80	0.70	0.70	1.00	1.0	1.04	2.59	5.08	1.04	85	75	75	95
iMPP2	0.70	0.80	1.00	0.70	1.0	2.59	1.56	1.04	5.08	75	85	95	75
iMPP3	1.00	0.70	0.70	0.80	1.0	1.04	2.59	5.08	1.56	95	75	75	85
iMPP4	0.70	1.00	0.80	0.70	1.0	5.08	1.04	1.56	2.59	75	95	85	75

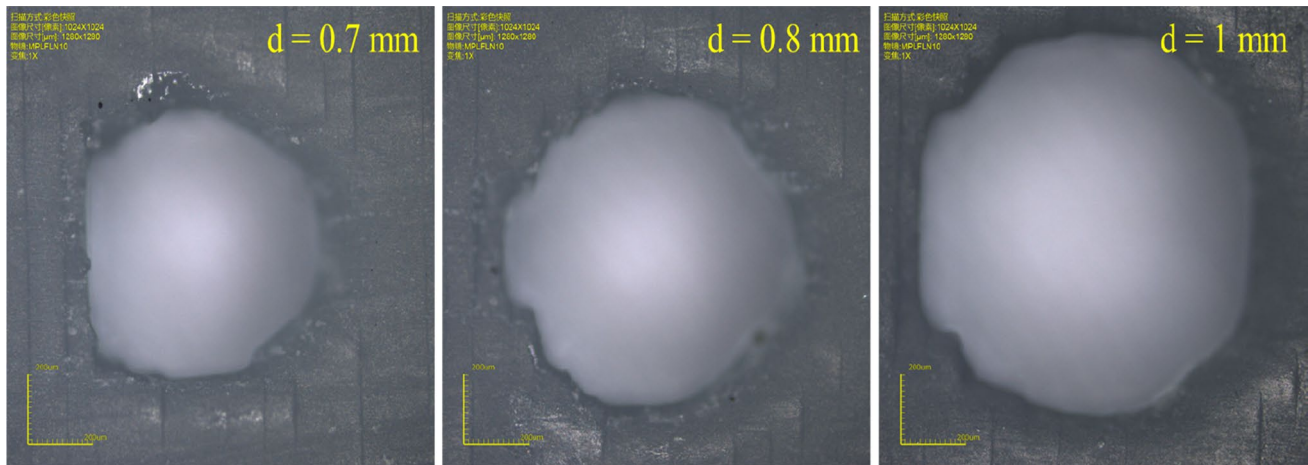


**Fig. 18** Detailed characterization of 3D printed samples using 3DMeasuring Laser Microscope

Similarly, Fig. 23 shows the verification between ECM-based predicted and FEM simulation results with that of experimentally measured results of sound absorption coefficients for four single-layer parallel-arranged iMPP1 ( $d_1=0.8$  mm,  $d_2=0.7$  mm,  $d_3=0.7$  mm,  $d_4=1.0$  mm) with partitioned same back-cavity depths. From Fig. 23a, when the back-cavity depth is 95 mm, it can be seen that the measured curve has good agreement with that of the predicted curve. However, the measured curve shows peaks between 201 and 401 Hz with an average absorption coefficient of  $\alpha = 0.92$ , which is slightly less than that of

ECM-based predicted and FEM simulation curves peaks of 185–395 Hz with an average absorption coefficient  $\alpha = 0.94$ . Nevertheless, ECM-based predicted, FEM simulation, and measured sound absorption coefficient values are in the close margin but definitely with a slight difference.

A similar trend can be seen for other values of back-cavity depths of 85 mm, 75 mm, and 50 mm as shown in Fig. 23b–d, respectively, which has further proved that the experimentally measured results are in good agreement with that of predicted and FEM simulation results. Overall, from the results of Fig. 23, it has been observed that as we

**Fig. 19** Liquid Crystal Display (LCD) technology-based 3D printed samples of Parallel-arranged iMPP: **a** iMPP with casing and partitioned multi-cavity **b** iMPP with casing and uniform cavity without partition

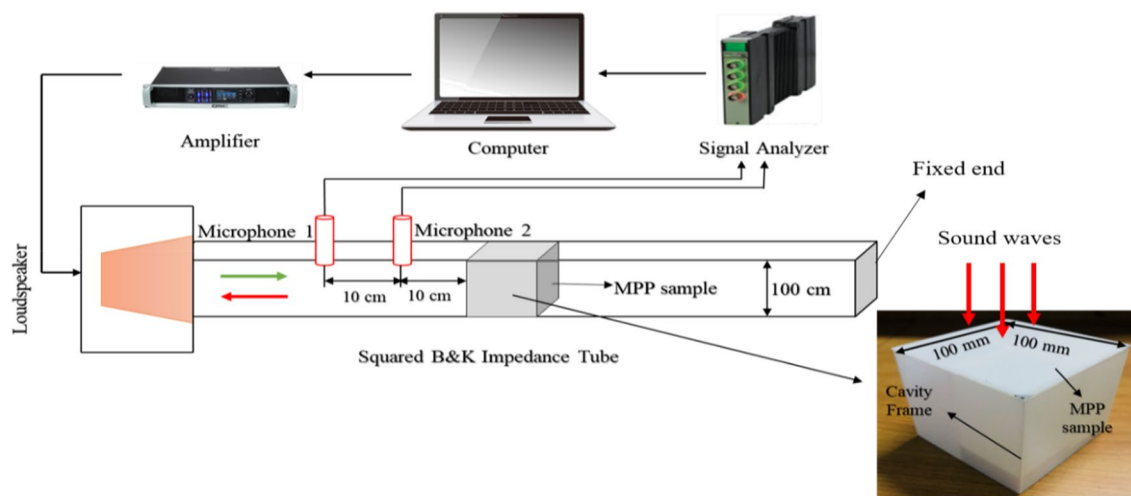
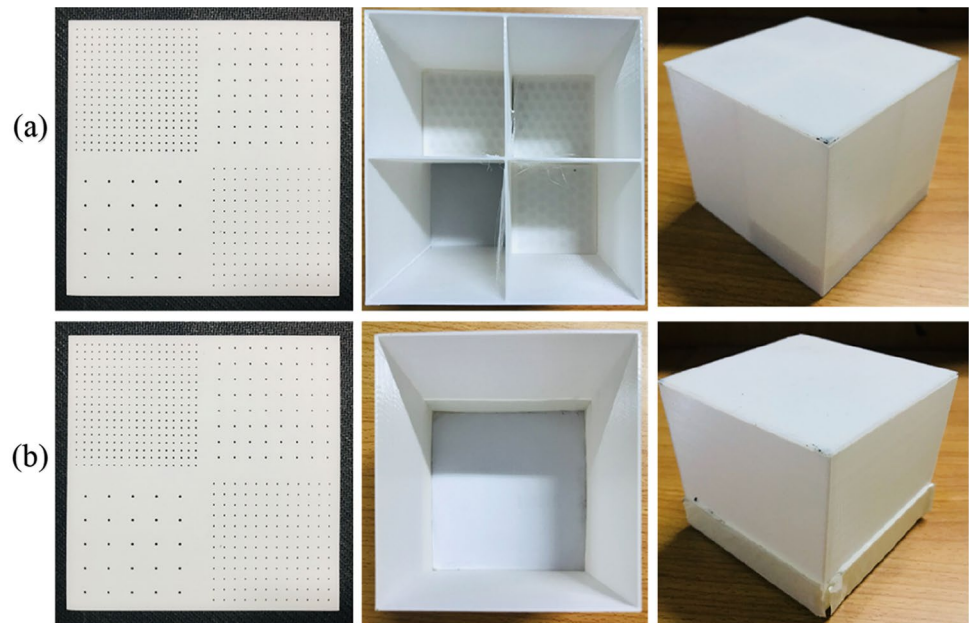


**Fig. 20** Schematic diagram of the absorption measurement system and the arrangement of the sample

increase the back-cavity depth of single-layer four parallel-arranged iMPP with uniform partitioned cavity depth, the curves move towards the low-frequency region with broader bandwidth and vice versa.

## 6 Conclusions

A four parallel-arranged single-layer iMPP absorber with sound absorption performance has been presented. Three different cases were discussed, i.e. the uniform cavity behind iMPP, the partitioned uniform cavity behind iMPP, and the partitioned multi-cavity behind iMPP. It is shown that

parallel-arrangement of inhomogeneous perforations with multi-cavity improves the absorption performance of MPP absorber in the low frequency compared to other homogeneous MPP. Parametric study by varying the perforation ratio, hole diameter, thickness, width and depth of cavity has been presented to evaluate the results obtained from each parameter changes in improving the absorption performance of iMPP. Further improvement in the low-frequency region can be accomplished by increasing the depth behind the sub-iMPP, having a big hole diameter with a small perforation ratio or a small hole diameter with a large perforation ratio. The Square impedance tube-based experiment is performed to validate the predicted and FEM simulation results,

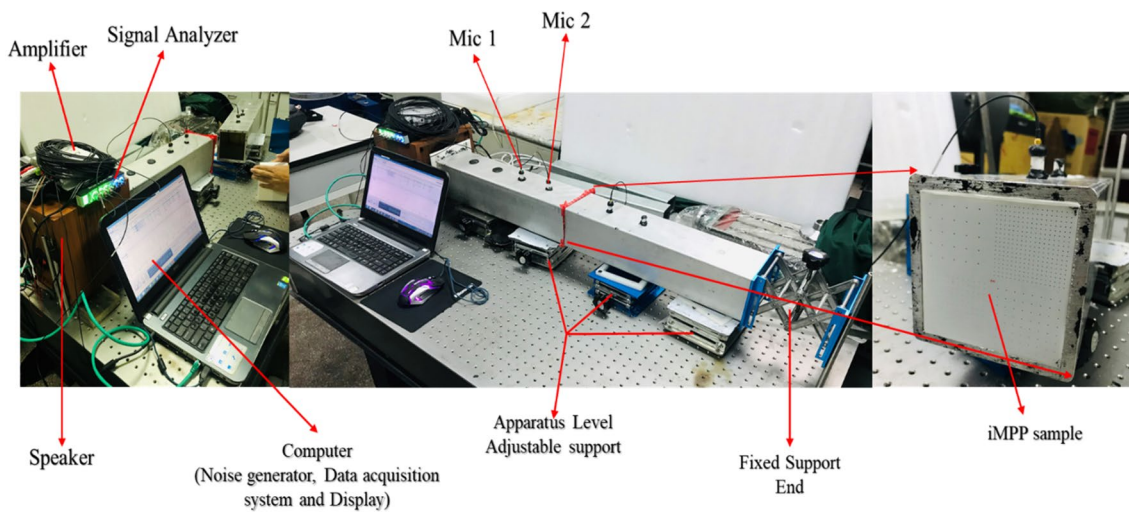


**Fig. 21** Square impedance tube experimental setup for the normal-incidence absorption coefficient measurement

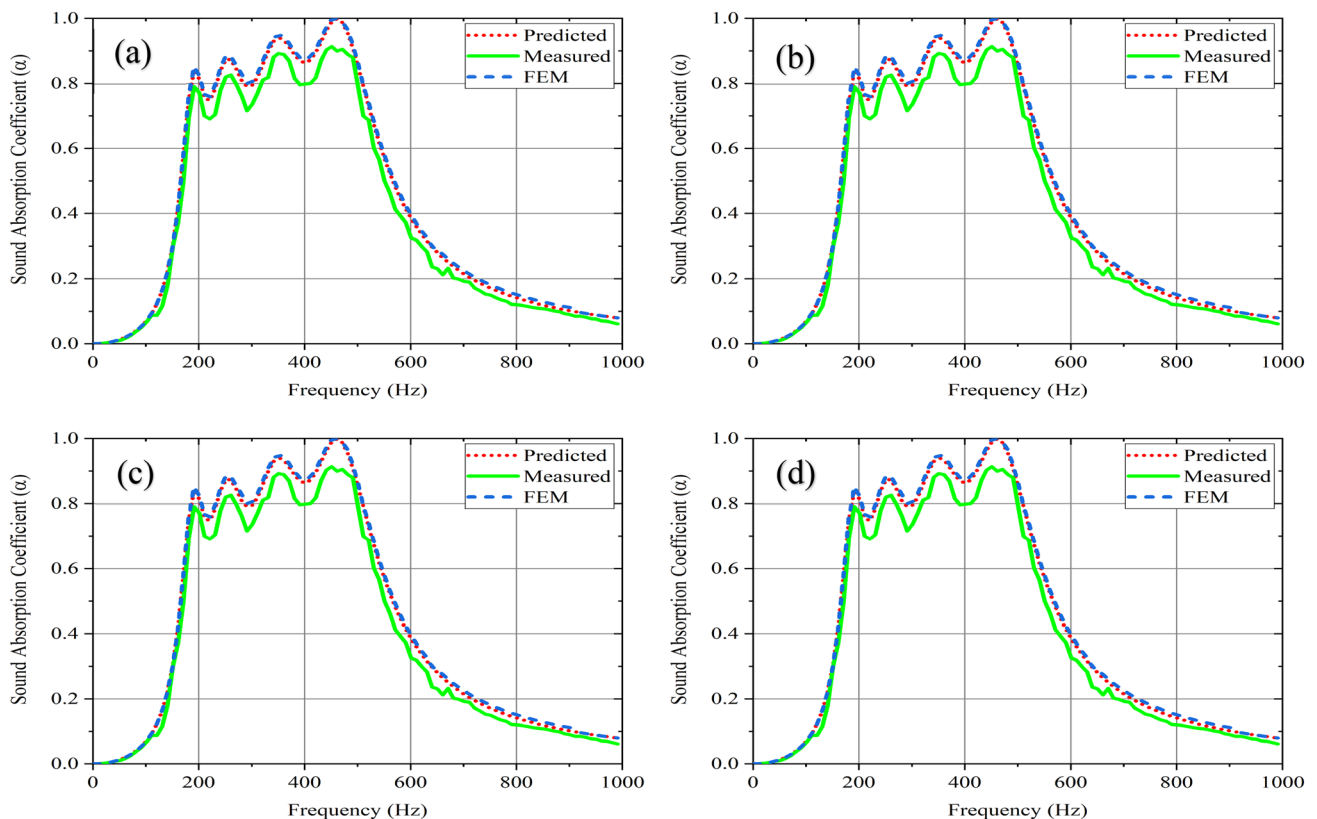


**Fig. 22** The sound absorption coefficient of a single layer of four parallel-arranged iMPPs with a partitioned multi-cavity depth. **a** iMPP1, **b** iMPP2, **c** iMPP3 and **d** iMPP4

proving to be in good agreement. Single-layer four parallel-arranged iMPPs with a partitioned, multi-cavity, thin structure have significantly wider sound absorption bandwidth and elevated absorption peaks than single-layer homogeneous MPPs. The results also show that the absorption

bandwidth in the low-frequency region increases with an increase in the back-cavity depth behind the iMPP and vice versa. The low-frequency region with a wider bandwidth of 195–455 Hz, an excellent average sound absorption peak of more than 90% ( $\alpha = 0.91$ ).

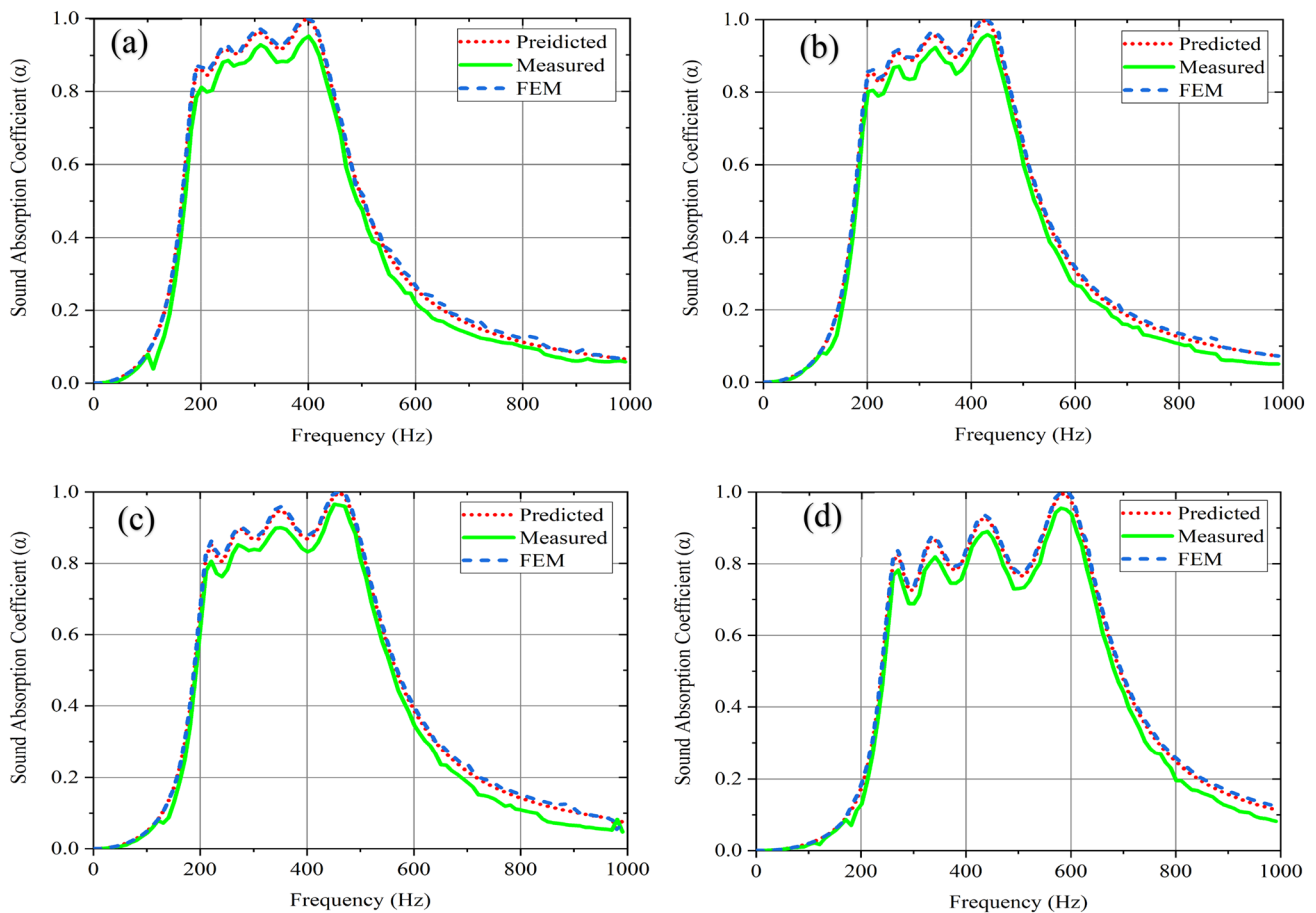


**Fig. 23** The sound absorption coefficient of a single-layer four parallel-arranged iMPPs with a partitioned same-cavity depth: **a**  $D=95$  mm, **b**  $D=85$  mm, **c**  $D=75$  mm, and **d**  $D=50$  mm

This particular study explains aspects of variations in aperture size, perforation ratio, and depth of cavity behind the iMPP layer, with and without partition. Similarly, this study is limited to the investigation of the normal incidence of the sound absorption coefficient. It can be further extended to sound absorption under field and oblique incidence and study the effect of the absorber size relative to the wavelength of the sound wave on the absorption performance.

**Acknowledgements** This work was supported by the National Natural Science Foundation of China (NSFC) under the Grant Nos. 51675401 and 51705395.

## References

- Dah-You, M.: Theory and design of microperforated panel sound-absorbing constructions. *Sci. Sin.* **18**, 55–71 (1975). <https://doi.org/10.1360/ya1975-18-1-55>
- Maa, D.Y.: Wide-band sound absorber based on microperforated panels. *Chin J Acoust* **4**, 3 (1985)
- Park, S.H.: Acoustic properties of micro-perforated panel absorbers backed by Helmholtz resonators for the improvement of low-frequency sound absorption. *J. Sound Vib.* **332**, 4895–4911 (2013). <https://doi.org/10.1016/j.jsv.2013.04.029>
- Zha, X., Kang, J., Zhang, T., Zhou, X.F.: Application approach for microperforated panel sound absorbers. *J. Chem. Inf. Model.* **19**, 258–269 (1994)
- Maa, D.Y.: Microperforated-panel wideband absorbers. *Noise Control Eng. J.* **29**, 77–84 (1987). <https://doi.org/10.3397/1.2827694>
- Sakagami, K., Morimoto, M., Koike, W.: A numerical study of double-leaf microperforated panel absorbers. *Appl. Acoust.* **67**, 609–619 (2006). <https://doi.org/10.1016/j.apacoust.2005.11.001>
- Sakagami, K., Matsutani, K., Morimoto, M.: Sound absorption of a double-leaf micro-perforated panel with an air-back cavity and a rigid-back wall: detailed analysis with a Helmholtz–Kirchhoff integral formulation. *Appl. Acoust.* **71**, 411–417 (2010). <https://doi.org/10.1016/j.apacoust.2009.11.014>
- Sakagami, K., Yairi, M., Morimoto, M.: Multiple-leaf sound absorbers with microperforated panels: An overview. In: 39th International Congress on Noise Control Engineering. 2010 (INTER-NOISE 2010), vol. 6, pp. 4859–4867 (2010)
- Sakagami, K., Nagayama, Y., Morimoto, M., Yairi, M.: Pilot study on wideband sound absorber obtained by combination of two different microperforated panel (MPP) absorbers. *Acoust. Sci. Technol.* **30**, 154–156 (2009). <https://doi.org/10.1250/ast.30.154>

10. Wang, C., Huang, L.: On the acoustic properties of parallel arrangement of multiple micro-perforated panel absorbers with different cavity depths. *J. Acoust. Soc. Am.* **130**, 208–218 (2011). <https://doi.org/10.1121/1.3596459>
11. Wang, C., Huang, L., Zhang, Y.: Oblique incidence sound absorption of parallel arrangement of multiple micro-perforated panel absorbers in a periodic pattern. *J. Sound Vib.* **333**, 6828–6842 (2014). <https://doi.org/10.1016/j.jsv.2014.08.009>
12. Liu, J., Herrin, D.W.: Enhancing micro-perforated panel attenuation by partitioning the adjoining cavity. *Appl. Acoust.* **71**, 120–127 (2010). <https://doi.org/10.1016/j.apacoust.2009.07.016>
13. Toyoda, M., Sakagami, K., Takahashi, D., Morimoto, M.: Effect of a honeycomb on the sound absorption characteristics of panel-type absorbers. *Appl. Acoust.* **72**, 943–948 (2011). <https://doi.org/10.1016/j.apacoust.2011.05.017>
14. Herdtle, T., Gerdes, R., Alexander, J.H., Bolton, J.S.: Transfer impedance of microperforated materials with tapered holes. In: 40th International Congress on Expo. Noise Control Engineering, 2011 (INTER-NOISE 2011), vol. 3, pp. 2005–2012 (2011). <https://doi.org/10.1121/1.4824968>
15. Qian, Y.J., Cui, K., Liu, S.M., Li, Z.B., Kong, D.Y., Sun, S.M.: Numerical study of the acoustic properties of micro-perforated panels with tapered hole. *Noise Control Eng. J.* **62**, 152–159 (2014). <https://doi.org/10.3397/1/376216>
16. Qian, Y.J., Kong, D.Y., Liu, S.M., Sun, S.M., Zhao, Z.: Investigation on micro-perforated panel absorber with ultra-micro perforations. *Appl. Acoust.* **74**, 931–935 (2013). <https://doi.org/10.1016/j.apacoust.2013.01.009>
17. Zhao, X., Fan, X.: Enhancing low frequency sound absorption of micro-perforated panel absorbers by using mechanical impedance plates. *Appl. Acoust.* **88**, 123–128 (2015). <https://doi.org/10.1016/j.apacoust.2014.08.015>
18. Li, D., Chang, D., Liu, B.: Enhanced low- to mid-frequency sound absorption using parallel-arranged perforated plates with extended tubes and porous material. *Appl. Acoust.* **127**, 316–323 (2017). <https://doi.org/10.1016/j.apacoust.2017.06.019>
19. Mosa, A.I., Putra, A., Ramlan, R., Prasetyo, I., Esraa, A.A.: Theoretical model of absorption coefficient of an inhomogeneous MPP absorber with multi-cavity depths. *Appl. Acoust.* **146**, 409–419 (2019). <https://doi.org/10.1016/j.apacoust.2018.11.002>
20. Li, X., Wu, Q., Kang, L., Liu, B.: Design of multiple parallel-arranged perforated panel absorbers for low frequency sound absorption. *Materials (Basel)*. **12**, 5–8 (2019). <https://doi.org/10.3390/ma12132099>
21. Li, L., Gang, X., Liu, Y., Zhang, X., Zhang, F.: Numerical simulations and experiments on thermal viscous power dissipation of perforated plates. *AIP Adv.* (2018). <https://doi.org/10.1063/1.5044705>
22. DIN E.: Iso 10534-2 Acoustics—Determination of sound absorption coefficient and impedance in impedance tubes—Part 2: Transfer-function method (2001)
23. Ho, K.M., Yang, Z., Zhang, X.X., Sheng, P.: Measurements of sound transmission through panels of locally resonant materials between impedance tubes. *Appl. Acoust.* **66**, 751–765 (2005). <https://doi.org/10.1016/j.apacoust.2004.11.005>

**Publisher's Note** Springer Nature remains neutral with regard to jurisdictional claims in published maps and institutional affiliations.